



HAL
open science

Very-long-chain fatty acids are involved in polar auxin transport and developmental patterning in Arabidopsis.

François Roudier, Lionel Gissot, Frédéric Beaudoin, Richard Haslam, Louise Michaelson, Jessica Marion, Diana Molino, Amparo Lima, Liên Bach, Halima Morin, et al.

► To cite this version:

François Roudier, Lionel Gissot, Frédéric Beaudoin, Richard Haslam, Louise Michaelson, et al.. Very-long-chain fatty acids are involved in polar auxin transport and developmental patterning in Arabidopsis.. *The Plant cell*, 2010, 22 (2), pp.364-75. 10.1105/tpc.109.071209 . hal-00856101

HAL Id: hal-00856101

<https://hal.science/hal-00856101>

Submitted on 31 May 2020

HAL is a multi-disciplinary open access archive for the deposit and dissemination of scientific research documents, whether they are published or not. The documents may come from teaching and research institutions in France or abroad, or from public or private research centers.

L'archive ouverte pluridisciplinaire **HAL**, est destinée au dépôt et à la diffusion de documents scientifiques de niveau recherche, publiés ou non, émanant des établissements d'enseignement et de recherche français ou étrangers, des laboratoires publics ou privés.

Very-Long-Chain Fatty Acids Are Involved in Polar Auxin Transport and Developmental Patterning in *Arabidopsis*

François Roudier, Lionel Gissot, Frédéric Beaudoin, Richard Haslam, Louise Michaelson, Jessica Marion, Diana Molino, Amparo Lima, Liên Bach, Halima Morin, Frédérique Tellier, Jean-Christophe Palauqui, Yannick Bellec, Charlotte Renne, Martine Miquel, Marco DaCosta, Julien Vignard, Christine Rochat, Jonathan E. Markham, Patrick Moreau, Johnathan Napier and Jean-Denis Faure
Plant Cell 2010;22;364-375; originally published online February 9, 2010;
DOI 10.1105/tpc.109.071209

This information is current as of October 2, 2013

Supplemental Data	http://www.plantcell.org/content/suppl/2010/02/02/tpc.109.071209.DC1.html
References	This article cites 66 articles, 37 of which can be accessed free at: http://www.plantcell.org/content/22/2/364.full.html#ref-list-1
Permissions	https://www.copyright.com/ccc/openurl.do?sid=pd_hw1532298X&issn=1532298X&WT.mc_id=pd_hw1532298X
eTOCs	Sign up for eTOCs at: http://www.plantcell.org/cgi/alerts/ctmain
CiteTrack Alerts	Sign up for CiteTrack Alerts at: http://www.plantcell.org/cgi/alerts/ctmain
Subscription Information	Subscription Information for <i>The Plant Cell</i> and <i>Plant Physiology</i> is available at: http://www.aspb.org/publications/subscriptions.cfm

Very-Long-Chain Fatty Acids Are Involved in Polar Auxin Transport and Developmental Patterning in *Arabidopsis* ^W

François Roudier,^{a,1} Lionel Gissot,^a Frédéric Beaudoin,^b Richard Haslam,^b Louise Michaelson,^b Jessica Marion,^{a,2} Diana Molino,^a Amparo Lima,^{a,3} Liên Bach,^a Halima Morin,^c Frédérique Tellier,^d Jean-Christophe Palauqui,^a Yannick Bellec,^a Charlotte Renne,^a Martine Miquel,^a Marco DaCosta,^{a,4} Julien Vignard,^a Christine Rochat,^a Jonathan E. Markham,^e Patrick Moreau,^f Johnathan Napier,^b and Jean-Denis Faure^{a,5}

^a Institut Jean-Pierre Bourgin, Unité Mixte de Recherche 1318, Institut National de la Recherche Agronomique-AgroParisTech, Centre de Versailles-Grignon, 78026 Versailles Cedex, France

^b Rothamsted Research, Harpenden, Herts AL5 2JQ, United Kingdom

^c Plateforme de Cytologie et d'Imagerie Végétale, Institut Jean-Pierre Bourgin, Institut National de la Recherche Agronomique, 78000 Versailles, France

^d Plateforme de Chimie du Végétale, Institut Jean-Pierre Bourgin, Institut National de la Recherche Agronomique, 78000 Versailles, France

^e Donald Danforth Plant Science Center, St. Louis, Missouri 63132

^f Laboratoire Biogenèse membranaire, Unité Mixte de Recherche 5200, Centre National de la Recherche Scientifique-Université Bordeaux 2, BP 33076 Bordeaux Cedex, France

Very-long-chain fatty acids (VLCFAs) are essential for many aspects of plant development and necessary for the synthesis of seed storage triacylglycerols, epicuticular waxes, and sphingolipids. Identification of the acetyl-CoA carboxylase PASTICCINO3 and the 3-hydroxy acyl-CoA dehydratase PASTICCINO2 revealed that VLCFAs are important for cell proliferation and tissue patterning. Here, we show that the immunophilin PASTICCINO1 (PAS1) is also required for VLCFA synthesis. Impairment of PAS1 function results in reduction of VLCFA levels that particularly affects the composition of sphingolipids, known to be important for cell polarity in animals. Moreover, PAS1 associates with several enzymes of the VLCFA elongase complex in the endoplasmic reticulum. The *pas1* mutants are deficient in lateral root formation and are characterized by an abnormal patterning of the embryo apex, which leads to defective cotyledon organogenesis. Our data indicate that in both tissues, defective organogenesis is associated with the mistargeting of the auxin efflux carrier PIN FORMED1 in specific cells, resulting in local alteration of polar auxin distribution. Furthermore, we show that exogenous VLCFAs rescue lateral root organogenesis and polar auxin distribution, indicating their direct involvement in these processes. Based on these data, we propose that PAS1 acts as a molecular scaffold for the fatty acid elongase complex in the endoplasmic reticulum and that the resulting VLCFAs are required for polar auxin transport and tissue patterning during plant development.

INTRODUCTION

Very-long-chain fatty acids (VLCFAs) are defined in plants as fatty acids with an acyl chain of at least 20 carbons in length. VLCFAs are components of seed storage triacylglycerols, cutic-

ular and epicuticular lipids, and sphingolipids. VLCFA synthesis requires four endoplasmic reticulum (ER)-bound enzymes constituting the elongase complex that carry out four sequential reactions: first, the condensation of a substrate acyl-CoA with malonyl-CoA catalyzed by ketoacyl-CoA synthase; second, the reduction of 3-ketoacyl-CoA by a ketoacyl-CoA reductase (KCR) followed by dehydration of the resulting 3-hydroxy acyl-CoA by the 3-hydroxy acyl-CoA dehydratase (PASTICCINO2 [PAS2]). The final enzymatic step is the reduction of the enoyl acyl-CoA by an enoyl-CoA reductase (ECR), resulting in an acyl-CoA that is two carbons longer (Zheng et al., 2005; Joubes et al., 2008). Malonyl-CoA is synthesized from acetyl-CoA by the cytosolic isoform of the acetyl-CoA carboxylase PAS3/GÜRKE (Baud et al., 2003, 2004). Loss of function of the 3-hydroxy acyl-CoA dehydratase PASTICCINO2 leads to embryo lethality, demonstrating that VLCFAs are essential for plant development (Bach et al., 2008). Reduction of VLCFA levels resulting from weak *pas3* or *pas2* alleles is also associated with abnormal development and ectopic cell proliferation (Faure et al., 1998). Loss of *Arabidopsis thaliana* ECR *CER10* function results in reduced

¹ Current address: Epigénétique et Epigénomique Végétale, Section Génomique Environnementale et Evolutive, Institut de Biologie de l'Ecole Normale Supérieure, Unité Mixte de Recherche 8197, Centre National de la Recherche Scientifique, 46 rue d'Ulm, 75230 Paris cedex 05, France.

² Institut des Sciences du Végétal, Centre National de la Recherche Scientifique, Avenue de la Terrasse, F-91198 Gif-sur-Yvette Cedex, France.

³ Department of Plant and Microbial Biology, University of California, Berkeley, CA 94720.

⁴ Laboratoire de Cytologie Expérimentale et Morphogenèse Végétale, Paris-VI, 94200 Ivry/Seine, France.

⁵ Address correspondence to faure@versailles.inra.fr.

The author responsible for distribution of materials integral to the findings presented in this article in accordance with the policy described in the Instructions for Authors (www.plantcell.org) is: Jean-Denis Faure (faure@versailles.inra.fr).

^W Online version contains Web-only data.

www.plantcell.org/cgi/doi/10.1105/tpc.109.071209

cell expansion and eventually in reduced size of aerial organs (Zheng et al., 2005). Similar observations were recently made upon RNA interference silencing of *Arabidopsis KCR* (Beaudoin et al., 2009). Overexpression of the condensing enzyme FATTY ELONGASE1 (FAE1) was found to alter chloroplast structure and cell shape, whereas an increase of the dehydratase activity leads to cell division and expansion defects (Millar and Kunst, 1997; Bach et al., 2008). Interestingly, ectopic expression of *FAE1* with the epidermal-specific promoter of *FIDDLEHEAD* results in trichome cell death (Reina-Pinto et al., 2009). Altogether these studies show that VLCFA homeostasis is essential and limiting for plant growth and development.

While the analysis of the role of VLCFAs in cell expansion could be explained by a deficit of essential lipids at the plasma membrane, the involvement of VLCFAs in cell proliferation and differentiation remains unclear. The *pas* mutants were initially identified as three complementation groups, *Pas1*, *Pas2*, and *Pas3*, showing ectopic cell proliferation in hypocotyls, cotyledons, and leaves. The *pas* mutations result in profound developmental alterations, which are already detectable during embryogenesis and lead to dwarf seedlings with short and thick hypocotyls and fused and misshapen leaves (Faure et al., 1998). The *pas* seedlings also show an increased competency for cell division in meristematic and differentiated cells that is enhanced by exogenous cytokinins and leads to callus-like development (Haberer et al., 2002; Harrar et al., 2003). Moreover, in these mutants, the shoot apical meristem is enlarged and shows an increased expression of meristematic markers (Haberer et al., 2002; Harrar et al., 2003). This higher proliferative activity is illustrated by the ability of the *pas2* mutation to rescue the *SHOOT MERISTEMLESS* mutant that is devoid of meristematic activity (Harrar et al., 2003). Finally, *PAS2* was found to interact in vitro with Cyclin-Dependent Kinase 1, suggesting that VLCFA synthesis might have a direct link with cell cycle progression (Da Costa et al., 2006). Cell fate acquisition is also altered in the *pas* mutants. The absence of cotyledon development in *pas3* (*gürke*) embryos is associated with overlapping cell fate territories within the apex (Kajiwara et al., 2004).

The identification of two *PAS* genes as essential enzymes of VLCFA biosynthesis suggest that the pleiotropic *pas* phenotype is directly associated with lipids that contain such acyl chains. However, the role of VLCFAs in cell fate acquisition and tissue patterning remains unclear, as does the involvement of *PAS1* in VLCFA synthesis. *PAS1* encodes a large molecular weight member of the immunophilin type FK506 binding protein family that have been reported in other eukaryotes to regulate the activity of many proteins involved in signaling pathways (Vittorioso et al., 1998; Harrar et al., 2001). In previous work, we have shown that *PAS1* interacts in vitro and in vivo through its C terminus with a member of the NAC family of transcription factors and regulates its subcellular localization (Smyczynski et al., 2006). Here, we show that the *pas1* mutant, similar to the two other *pas* mutants, has reduced levels of VLCFAs and that *PAS1* interacts in the ER with the core elongase components, suggesting a new role of the immunophilin in scaffolding the fatty acid elongase complex. We also show that the impairment of *PAS1* function results, like in *pas3*, in defective cotyledon formation associated with an altered patterning of the embryo apex. We

provide evidence that this morphological defect and the absence of lateral root initiation later in development are associated with alterations in auxin response, resulting from a lack of polar targeting of the auxin efflux carrier PIN1. In *pas1*, defective PIN1 polar targeting is correlated with hypersensitivity to the trafficking inhibitor brefeldin A. Fatty acids are directly involved in polar auxin transport since exogenous application of lipids restore auxin distribution in lateral roots. Based on these data, we propose that *PAS1* is involved in fatty acid elongation and that the resulting VLCFAs are essential regulators of cell differentiation during development by regulating polar auxin distribution.

RESULTS

PAS1 Is Required for VLCFA Accumulation in Triacylglycerols, Free Fatty Acids, and Sphingolipids

The fact that the three *pas* mutants share similar phenotypes and that both *PAS2* and *PAS3* are essential for VLCFA synthesis (Baud et al., 2003, 2004; Bach et al., 2008) prompted us to determine whether the *pas1-3* mutant was also altered in lipid metabolism. Quantification of VLCFA content in *pas1-3* mature seeds revealed that the levels of 20:2 and 22:1 fatty acids were reduced by 50% compared with wild-type levels and that, conversely, the level of short-chain 16:0 and 18:1 fatty acids showed a 40% increase (Figure 1A). Similar changes in the levels of 20:1 and 22:1 but also 16:0 were observed in weak *pas2* and *pas3* alleles (Baud et al., 2004; Bach et al., 2008). VLCFA levels in *pas1* roots were also reduced by 38, 42, and 60% for 22:0, 22:1, and 24:0, respectively (Figure 1B). VLCFAs are also found in sphingolipids (Dunn et al., 2004). Contrary to seed triacylglycerols, sphingolipids are essential for embryo development (Chen et al., 2006). Sphingolipids are composed of a long-chain base (amino alcohol) and an amide linked with a fatty acyl chain (Dunn et al., 2004). These lipids are characterized by the acyl chain length and its degree of unsaturation, as well as the nature of the polar head group, which can be modified by glycosylation and phosphorylation. Like *pas2-1*, both *pas1-3* and *pas3-1* mutants were affected in sphingolipid content showing a lower amount of very-long-chain (C_{24} and C_{26}) sphingolipids, which are the predominant forms in *Arabidopsis* (Figure 1C) (Bach et al., 2008).

Specific Sphingolipid Modifications Are Associated with Altered *PAS1* Function

Reduction of C_{24} and C_{26} sphingolipids in *pas1-3* and *pas3-1* was associated with lower levels of Δ^8 -unsaturated long-chain-base moieties 8-sphingenine (d18:1⁸) and 4-hydroxy-8-sphingenine (t18:1⁸), likely due to modifications of the different classes of sphingolipids (Borner et al., 2005; Markham et al., 2006; Chen et al., 2008) (see Supplemental Figure 1A online). To assess whether *PAS1* targets specific classes of sphingolipids, we performed a complete sphingolipid profiling of both mutants. The levels of simple sphingolipids like Ceramide (Cer) were increased by ~30 and 20% for *pas1-3* and *pas3-1*, respectively, whereas hydroxyceramide levels increased (by ~30%) only in *pas1-3* (see Supplemental Figure 1B online). Global increase of

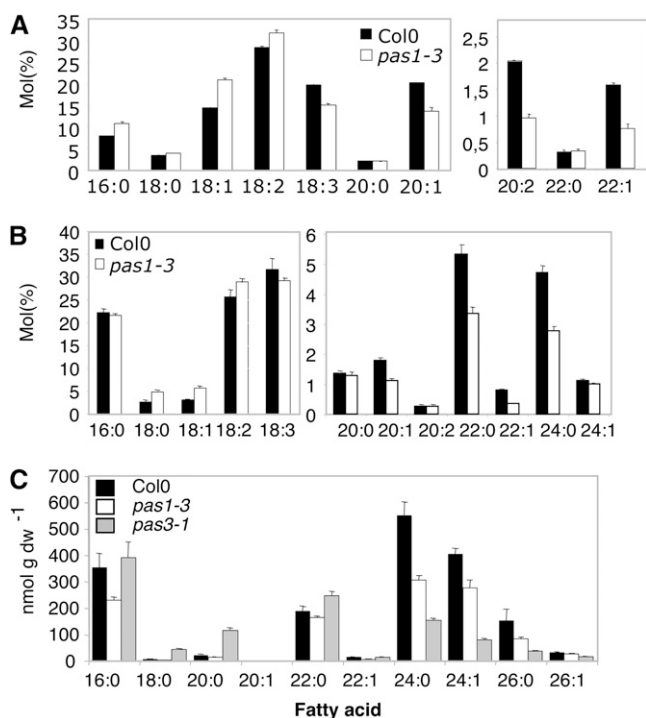


Figure 1. Lipids with Very Long Acyl Chains Are Altered in *pas1-3* and *pas3-1* Mutants.

(A) Triacylglycerol composition of wild-type (Col-0; black bars) and *pas1-3* seeds (white bars).

(B) Total fatty acid composition of wild-type (Col-0; black bars) and *pas1-3* mutant 10-d-old roots (white bars).

(C) Sphingolipid composition of wild-type (Col-0; black bars), *pas1-3* (white bars), and *pas3-1* (gray bars) seedlings.

Data represents the mean of three independent analyses. Error bar indicates SE.

Cer in both mutants was mainly caused by the accumulation of long-chain 16:0-Cer (see Supplemental Figure 2 online), whereas the very-long-chain 24:0- and 26:0-Cer levels were substantially reduced in *pas3-1* and decreased only modestly in *pas1-3* (see Supplemental Figure 2 online). We then examined the complex glycosylated sphingolipids glucosyl inositol phosphoryl ceramide (GIPC) and glucosyl ceramide (GluCer). GIPCs levels were not significantly modified in *pas3-1* and were slightly reduced in *pas1-3* (~25% decrease). Contrary to GIPCs, GluCer levels were reduced by ~50 and 63%, respectively, for *pas1-3* and *pas3-1* mutants (see Supplemental Figure 1C online). Very-long (C_{20+}) and long-chain (C_{18-20}) GluCers were specifically reduced (see Supplemental Figure 2 online). Reduction of GluCer levels could result from either a decrease in synthesis or a higher turnover rate (by specific hydrolases). To discriminate between these two possibilities, GluCer synthesis was measured by ¹⁴C-acetate incorporation followed by extraction of this sphingolipid fraction. GluCer labeling in *pas1-3* and *pas3-1* was strongly reduced compared with the wild type, demonstrating that synthesis of GluCer was impaired in both mutants (see Supplemental Figure 1D online). Mutations affecting biosynthesis of sterols, which are associated with sphingolipids in membrane domains, also lead

to strong developmental modifications especially during embryogenesis (Schaller, 2004). Contrary to VLCFAs, the levels of sterol glycosides were not modified and the levels of sterol were even increased in both *pas1-3* and *pas3-1* mutants compared with the wild type (see Supplemental Table 1 online). In conclusion, the *pas1-3* mutant is characterized by a specific reduction of VLCFAs like for the other *pas* mutants, the 3-hydroxyacyl-CoA dehydratase *pas2*, and the cytosolic acetyl CoA carboxylase *pas3*.

PAS1 Associates with the VLCFA Elongase Complex in the ER

PAS1 is a member of the immunophilin family known in animals and plants to target protein complexes and to regulate their assembly or activities (Barik, 2006; Bouchard et al., 2006; Fu et al., 2007). An attractive hypothesis to explain the decrease in VLCFAs would be that PAS1 interacts directly with the VLCFA elongase complex in the ER. PAS1 was originally described to accumulate in the cytosolic space but was also found in the nucleus upon auxin-induced dedifferentiation (Smoczynski et al., 2006). Detailed analysis of the distribution of a green fluorescent protein (GFP)-PAS1 fusion showed that it was mainly associated with the ER as confirmed by its colocalization with the CD3-959 marker (Figure 2A). The four enzymes forming the elongase complex are all localized in the ER (Zheng et al., 2005; Bach et al., 2008; Joubes et al., 2008). To probe direct interactions between PAS1 and members of the elongase complex, we used bimolecular fluorescence complementation (BiFC). The different genes were cloned in frame with the N- or C-terminal half of yellow fluorescent protein (YFP), and the different combinations were then tested in transient assays (Desprez et al., 2007; Marion et al., 2008). YFP fluorescence was detected for all the combinations involving PAS1 and the elongase complex core members KCR, PAS2, and ECR (Figures 2B and 2D). In this assay, the interaction between the elongase complex core members KCR, PAS2, and CER10 was used as a positive control (Bach et al., 2008) (Figure 2B, right). Conversely, no interaction was detected between PAS1, KCR, or CER10 and the ER-localized enzymes DPL1 and SBH2, involved in sphingolipid long chain base metabolism (Figure 2C; see Supplemental Figure 3C online; Tsegaye et al., 2007; Chen et al., 2008), demonstrating the specificity of interaction between PAS1 and the elongase core enzymes. PAS1 interaction with the core elongase component PAS2 was confirmed by pull down of either PAS1-GFP expressed in BY2 cell culture using a His₆-PAS2 affinity column or radiolabeled in vitro-translated PAS2 using a His₆-PAS1 affinity column (see Supplemental Figures 3A and 3B online). Interaction of PAS1 with the elongase enzymes in the ER was shown by colocalizing the YFP^N-CER10/YFP^C-PAS1 fusion protein with the ER marker CD3-959 (Figure 2D). Altogether, these data demonstrate that PAS1 is associated in the ER with the VLCFA elongase complex and thus is directly linked to VLCFA synthesis, as PAS2 and PAS3 are.

PAS1 Is Involved in Cotyledon Development during Embryogenesis

The fact that the three *pas* mutants are severely altered in their development raises the question of the role of VLCFAs in cell

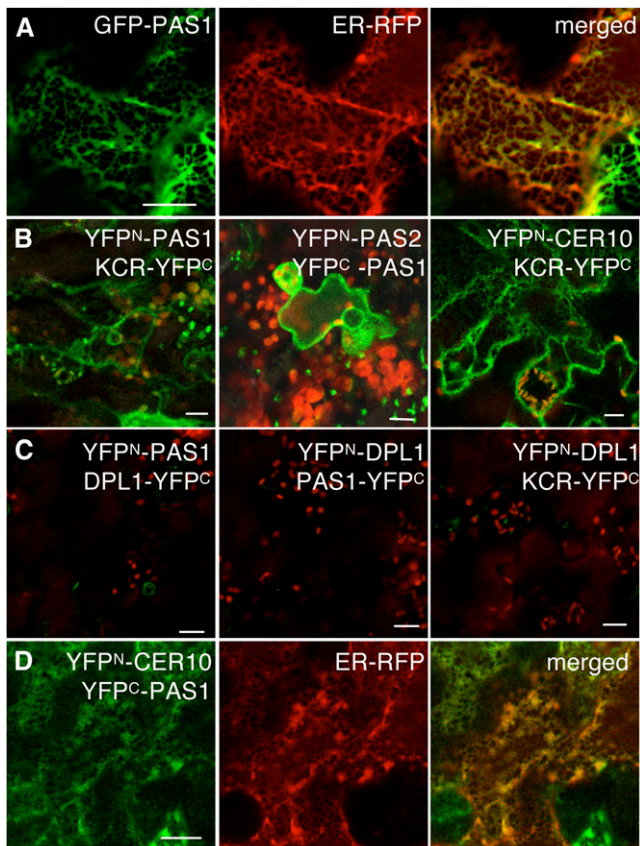


Figure 2. PAS1 Interacts with Elongase Enzymes in the ER of *Arabidopsis* Epidermal Cells.

- (A) Coexpression of *35S::GFP-PAS1* (left) and ER marker CD3-959:mCherry (middle) showed colocalization (merged, right).
- (B) Coexpression of the split YFP pairs YFP^N-PAS1/KCR-YFP^C, YFP^N-PAS2/ YFP^C-PAS1, and YFP^N-CER10/KCR-YFP^C led to BiFC of YFP (green). Chloroplast autofluorescence is red.
- (C) Coexpression of split YFP pairs YFP^N-PAS1/ YFP^C-DPL1, YFP^N-DPL1/ YFP^C-PAS1, and YFP^N-CER10/YFP^C-DPL1 did not produce any YFP fluorescence.
- (D) Coexpression of YFP^N-CER10/YFP^C-PAS1 *GFP* (left) and ER marker CD3-959:mCherry (middle) showed BiFC colocalization in the ER (merged, right).
- Bars = 10 μ m in (A) to (C) and 40 μ m in (D).

proliferation and differentiation. We first characterized the cellular basis of the *pas1* phenotype during early stages of development. Mutations in the *PAS1* gene lead to seedlings with short hypocotyls and reduced cotyledon growth. These phenotypic alterations were already observed in 25% of the mature embryos present in siliques from heterozygous *pas1/+* plants (Faure et al., 1998) and ranged from aborted growth (fox-head shape) to complete loss of cotyledons (almond shape) (Figure 3A; see Supplemental Figure 4 online). The remaining embryos (+/+ and *pas1/+*) were phenotypically indistinguishable, confirming that *pas1-3* was fully recessive (Faure et al., 1998) and will be referred to phenotypically as wild type. Morphological analysis of embryogenesis revealed that at the heart stage, mutant embryos are

characterized by a flattened apex with larger hypocotyls (Figure 3A) and the accumulation of starch granules (Figure 3A; see Supplemental Figure 4 online). In comparison with the wild type, the protodermis of the mutant apex showed uncoordinated division planes resulting in severe loss of planar polarity. Interestingly, L1 cells displayed heterogeneous shapes, suggesting that epidermal polarity is altered at the single cell level (Figure 3A). We previously showed that *PAS1* is expressed mostly in cotyledons of mature embryos (Smyczynski et al., 2006). In situ hybridizations revealed that *PAS1* showed enhanced expression in cotyledons during late developmental stages (Figure 3B). The *PAS1* expression pattern is therefore in agreement with the phenotypic defect observed during *pas1* embryo development.

PAS1 Is Required for Apex Patterning of the Embryo

To understand better the phenotypic alterations observed in mutant embryos, different cellular markers were introduced into the *pas1-3* mutant. Expression analysis of the mitotic marker *pCYCB1;1::db- β -glucuronidase* (*GUS*) (Colon-Carmona et al., 1999) revealed no obvious differences in mitotic patterns between wild-type and *pas1-3* embryos (see Supplemental Figure 5 online). However, several cell identity markers representative of specific domains in the embryo apex showed abnormal expression patterns. The expression domain of *WUSCHEL* (*WUS*), which characterizes the organizing center of the apical meristem and is normally restricted to two cells in wild-type embryos, was clearly enlarged, encompassing up to 10 cells in the *pas1* embryo. This is in agreement with the enhanced expression of the whole KNAT gene family that was observed in the different *pas* mutants (Harrar et al., 2003). The extension of the *WUS* expression in *pas1* was generated by contiguous cells still defining a stem cell niche (Figure 3C) or by cells scattered into the apical domain of the embryo (see Supplemental Figure 6 online). The *WUS* domain is normally limited by the expression of *CUP SHAPE COTYLEDON2* (*CUC2*), which defines the boundaries between the cotyledons and the central domain of the meristem (Figure 3C). In *pas1-3* embryos, *CUC2* expression was not restricted to boundary domains but expanded throughout the entire apical domain. Similarly, *AINTEGUMENTA*, which marks cotyledon primordia, showed an enlarged expression zone spreading throughout the entire apical part of *pas1-3* embryos (Figure 3C). Thus, in the apex of *pas1-3* embryos, the different cell territories required for proper organogenesis strongly overlap, leading to the coexistence of otherwise mutually exclusive cell fates. In the most severe cases (5% of homozygous *pas1* embryos), this aberrant apex patterning resulted in the total absence of cotyledon development and the lack of bilateral symmetry.

Defective Cotyledon Development in *pas1* Is Associated with Modified Polar Auxin Patterning

Cotyledon development is associated with dynamic auxin mobilization with an auxin response restricted to the globular embryo hypophysis at first, followed by a redistribution of the response toward the apical domain and in the cotyledon domains at the triangular and heart stages (Aida et al., 2002; Benkova et al., 2003; Furutani et al., 2004; Trembl et al., 2005;

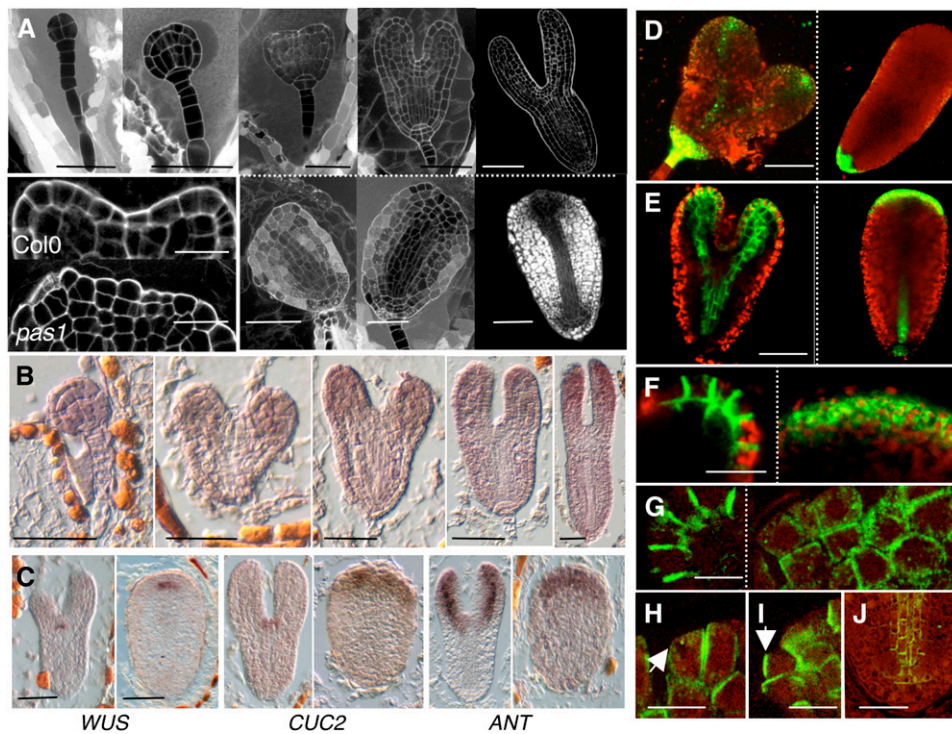


Figure 3. PAS1 Is Required for Cell Patterning and Polarity in the Embryo Apex.

(A) Development of wild-type (top row) embryo at the dermatogen, globular, heart, torpedo, and late torpedo stage, respectively (from left to right). The first phenotypic alteration in *pas1-3* embryos is visible at the heart stage with the absence of cotyledon formation (bottom row). Mutant embryos (bottom) were taken at the same respective stage (i.e., from the same silique) as the wild type (top row). Apical cells of *pas1* embryos have lost their polar growth (inset, bottom) compared with the wild type (inset, top). Embryos were fixed and stained with propidium iodide.

(B) In situ hybridization of *PAS1* mRNA during embryo development in the wild type. Embryos were taken at globular, young heart, late heart, young torpedo, and late torpedo stages (left to right).

(C) In situ hybridization of *WUS*, *CUC2*, and *ANTEGUMENTA (ANT)* mRNA in wild-type (left panel of each pair) and *pas1-3* (right panel of each pair) embryos. Bars = 40 μm except for the inset in **(A)**, which is 10 μm .

(D) pDR5-GFP distribution in the wild type (left) and *pas1-3* mutant (right).

(E) pPIN1:PIN1-GFP distribution in the wild type (left) and *pas1-3* mutant (right).

(F) Detail of pPIN1:PIN1-GFP distribution in the tip of a wild-type cotyledon (left) and the apex of *pas1-3* embryo (right) at heart stage.

(G) to (J) Immunolocalization of PIN1 in wild-type and *pas1-3* embryos.

(G) Detail of PIN1 distribution in the tip of a wild-type cotyledon (left) and in the apex of the *pas1-3* mutant where aggregates are visible (right).

(H) and **(I)** Altered polar distribution of PIN1 in the apex of the *pas1-3* mutant with PIN1 localizations facing each other in adjacent cells (**(H)**, arrow) or facing outward (**(I)**, arrow).

(J) PIN1 polarity is normal in *pas1-3* provascular and root pole cells.

Bars = 40 μm in **(D)** and **(E)**, 20 μm in **(F)**, 10 μm in **(G)** to **(I)**, and 30 μm in **(J)**.

Izhaki and Bowman, 2007). To monitor auxin response during cotyledon development, we introduced the synthetic auxin-responsive promoter *DR5* driving the GFP reporter gene in *pas1*. As reported previously, wild-type torpedo embryos showed *DR5* expression at the root pole, at the tip of the cotyledons, and in the vascular tissues (Friml et al., 2003). By contrast, *DR5* expression was detected only at the root pole in *pas1* (Figure 3D). No *DR5* expression could be detected in the apical domain or the vascular tissues of *pas1*, suggesting that auxin was not properly redistributed. Auxin distribution in the embryo involves specific polar influx and efflux carriers (Jenik and Barton, 2005). In particular, the PIN1 efflux carrier is involved in downward auxin transport through the vascular tissues to the

root pole and in upward auxin transport through epidermal cells from the hypophysis to the cotyledon tips. In order to determine whether the altered distribution of auxin observed in *pas1-3* could be associated with a defect in polar auxin transport, PIN1 expression and subcellular localization were investigated with a PIN1-GFP fusion driven by the PIN1 promoter. In *pas1-3*, expression of the pPIN1:PIN1-GFP construct was observed in both epidermal and vascular cells of the embryo, like in the wild type (Figure 3E). However, whereas PIN1-GFP was localized in the lateral membranes of epidermal cells in wild-type embryos (Figure 3F, left), its subcellular distribution was often diffused or aggregated inside *pas1* epidermal cells (Figure 3F, right). Immunolocalization analysis confirmed the defective polar distribution of

PIN1 in *pas1-3* apical cells, where it was found aggregated in the cell and showed no clear polar organization when present at the plasma membrane (Figure 3G, right). For instance, PIN1 was observed in contiguous lateral membranes of two adjacent epidermal cells or in the outward membrane facing the inner seed cavity (Figures 3H and 3I, arrows). The alteration of PIN1 polar localization in *pas1-3* could already be observed at the late globular stage before any detectable changes in morphology, suggesting that impaired auxin distribution is likely the cause of the subsequent patterning defects observed in the *pas1-3* embryo (see Supplemental Figure 7 online). In agreement with the specific expression of *PAS1* at the embryo apex, loss of polar distribution of PIN1 was restricted to the apical domain of *pas1-3* embryo but was not modified in vascular cells of the hypocotyl and did not affect *DR5* expression at the root pole (Figures 3D and 3J). Moreover, similar alterations were observed in embryos of the VLCFA biosynthetic mutant *pas3-1* (see Supplemental Figure 8 online), indicating that *pas1-3* auxin transport defects were also linked with reduced VLCFA levels. In conclusion, the patterning defects observed in the apical domain of *pas1* embryos were associated with abnormal polar distribution of PIN1 and compromised auxin response due to defective VLCFA synthesis.

PAS1 Is Involved in Lateral Root Development

Since *PAS1* is also expressed during postembryonic development, we investigated whether other developmental defects observed in *pas1* seedlings could also be related to altered polar auxin distribution. The *pas1-3* mutant was characterized by the absence of lateral root development (see Supplemental Figure 9A online; Faure et al., 1998; Vittorioso et al., 1998), the initiation of which is strongly dependent on local auxin accumulation in pericycle, cortex, and epidermal cells (Benkova et al., 2003; Tanaka et al., 2006). In primary and lateral roots, *PAS1* was found to be specifically expressed in the meristem and the columella cells but not in the elongation or differentiation zones (see Supplemental Figure 9B online). *PAS1* was expressed at the initial stage of lateral root formation where periclinal division of pericycle cells is observed, and its expression was maintained mostly at the tip of the root primordia until meristem formation (see Supplemental Figure 9C online). Analysis of *DR5:GFP* expression indicated that auxin response in *pas1-3* primary roots and during the early steps of lateral root initiation was similar to the wild type (Figure 4A; see Supplemental Figure 10A online). However, *DR5* expression was rarely detected in the outer cortical cells and never observed in epidermal cells during lateral root formation (Figure 4B). In some instances, *pas1-3* mutants produced a few degenerative lateral root primordia with weak or no *DR5* expression (Figures 4C and 4K) that never developed into lateral roots with proper columella and vascular *DR5* expression (see Supplemental Figure 11 online). Thus, as in embryo apex patterning, de novo organogenesis is compromised in *pas1* roots.

Defective Lateral Root Development in *pas1* Is Associated with Altered Polar Auxin Transport

Auxin distribution during primary and lateral root development is associated with specific expression patterns of PIN1

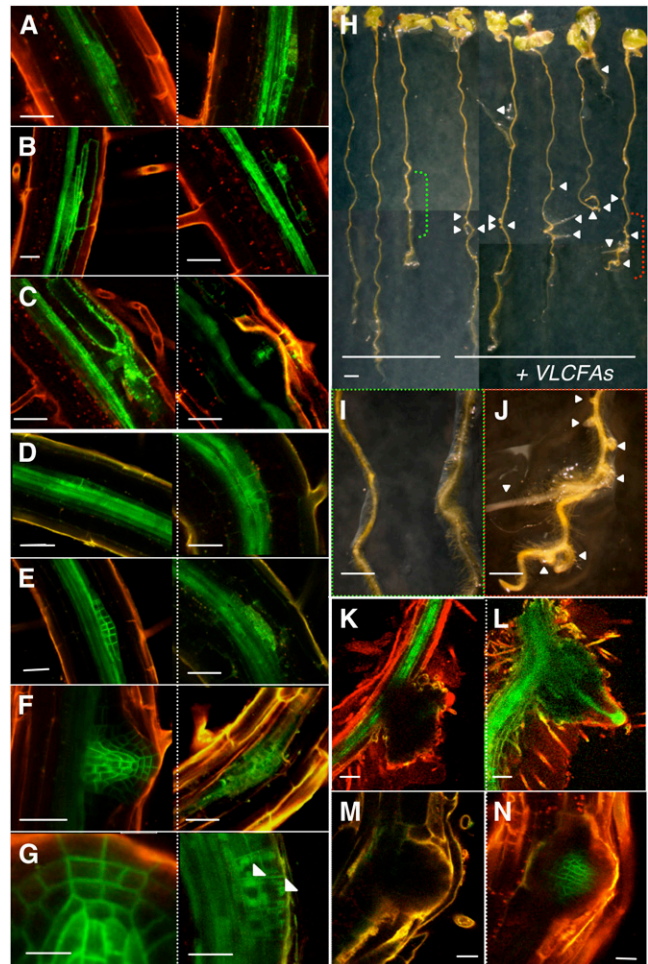


Figure 4. VLCFAs Are Involved in Lateral Root Development and Auxin Polar Distribution.

(A) to (G) *pDR5:GFP* [(A) to (C)] and *pPIN1:PIN1-GFP* [(D) to (G)] expression during sequential steps of lateral root development in the wild type (left) and the *pas1-3* mutant (right). In the *pas1* mutant, PIN1-GFP was found accumulated inside primordia cells [(E) to (G), right] often in aggregates [(G), arrows].

(H) to (J) Exogenous application of VLCFAs restored lateral root development in *pas1-3* mutants. Seedlings were grown in presence [(H), right] or absence [(H), left] of 200 μ M fatty acids (18:0, 20:0, 22:0, and 24:0). Details of control [(I), green bracket in (H)] or treated roots [(J), red bracket in (H)] are shown. Arrows point to lateral root outgrowth in the *pas1-3* mutant [(H) and (J)].

(K) to (N) VLCFA application restores polar auxin transport in *pas1-3* lateral roots. Normal *pDR5:GFP* [(K) and (L)] and *pPIN1:PIN1-GFP* [(M) and (N)] expression patterns were observed in treated *pas1-3* lateral root tips [(L) and (N)] but not in untreated mutant roots [(K) and (M)].

Bars = 45 μ m in (A) to (F), 30 μ m in (G) (left), 20 μ m in (G) (right), 1 mm in (H), 300 μ m in (I) and (J), and 20 μ m in (K) to (N).

(Benkova et al., 2003; Tanaka et al., 2006). In the primary root, PIN1 distribution was similar between the wild type and the mutant, except that *pas1-3* showed a higher occurrence of cytosolic PIN1:GFP aggregates (Figure 5; see Supplemental Figure 10B online). During the initial steps of lateral root

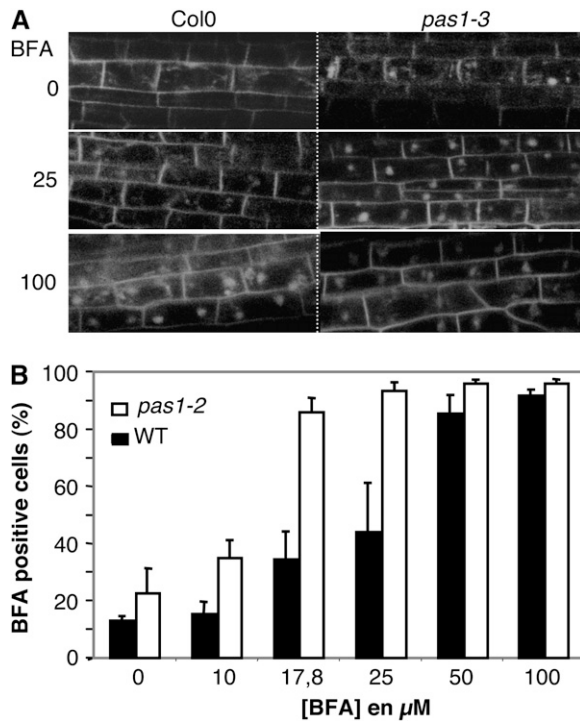


Figure 5. BFA-Dependent PIN1-GFP Aggregation Is Enhanced in *pas1* Mutant Cells.

(A) BFA induction of PIN1-GFP aggregation in *pas1*. In contrast with the wild type (left), PIN1-GFP aggregation can be observed in the *pas1-3* mutant (right) even in the absence of BFA (0 μM) and is strongly enhanced with 25 μM BFA treatment.

(B) The *pas1-3* mutation enhances sensitivity to BFA. The relative number of vascular cells showing BFA compartments as illustrated in **(A)** at 100 μM was monitored in the wild type and *pas1* according to the BFA concentration. Data are the mean of three replicates of 25 roots \pm SE.

initiation, PIN1 expression was clearly visible in the newly divided pericycle cells for both wild-type and *pas1-3* roots (Figure 4D, right). At the stage of the first periclinal divisions of the primordia, PIN1:GFP was not sharply localized to the plasma membrane as in the wild type (Figures 4E and 4F, right) but showed diffused or aggregated accumulation in the cell (Figure 4G, right). Interestingly, the influx carrier AUX1, which is also expressed during the early steps of lateral root development, was properly targeted to the plasma membrane in the *pas1-3* mutant (see Supplemental Figures 10C to 10G online). In conclusion, defective organ formation in *pas1* embryos and roots was associated with specific PIN1 mistargeting leading to altered auxin distribution.

BFA Sensitivity of PIN1 Distribution Is Enhanced in *pas1*

Polar localization of PIN1 results from a continuous turnover of the protein from the plasma membrane to endosomal compartments (Geldner et al., 2001, 2003; Grebe et al., 2003; Muday et al., 2003; Boutte et al., 2006; Jaillais et al., 2006). The lower

VLCFA levels in *pas1-3* mutant cells could result in an altered trafficking of PIN1 and its subsequent accumulation in the cytosol. In order to test this hypothesis, we used brefeldin A (BFA), which inhibits anterograde (toward the plasma membrane) trafficking of PIN1 by affecting the activity of GNOM, a small G protein member of the GTP/GDP exchange factor family (Steinmann et al., 1999). In the wild type, BFA treatment results in the accumulation of PIN1 in large endosomal and Golgi compartments called BFA compartments (Boutte et al., 2006) and thus provides an interesting tool to monitor PIN1 trafficking. The sensitivity of PIN1 distribution to increasing concentrations of BFA was investigated in wild-type and *pas1-3* primary roots. BFA was applied to wild-type and *pas1-3* seedlings for 30 min, and the occurrence of PIN1:GFP in large BFA compartments was monitored in stele cells (Figure 5A). BFA (100 μM) led to the formation of BFA compartments of PIN1:GFP in most cells in wild-type seedlings, whereas 25 μM affected \sim 50% of the cells (Figure 5B). On the contrary, *pas1-3* mutant cells showed saturating BFA responses already at 25 μM , and $>$ 80% cells were BFA responsive at 17.8 μM (compared with 30% in the wild type), indicating that PIN1 localization was more sensitive to BFA in the *pas1-3* background. This increased sensitivity of PIN1 localization to BFA suggests that PAS1, probably via the synthesis of VLCFAs, modifies protein recycling.

VLCFAs Are Required for Auxin Distribution and for Lateral Root Development

Finally, to demonstrate the role of VLCFAs in both auxin distribution and lateral root development, *pas1* mutants expressing *pDR5:GFP* or *pPIN1:PIN1-GFP* were directly grown in the presence or absence of a mixture of VLCFAs (18:0, 20:0, 22:0, and 24:0). After 4 d of treatment, no significant differences could be observed for wild-type roots (data not shown). However, VLCFA treatment enhanced lateral root development in *pas1-3* compared with the wild type (Figures 4I and 4J). While only 2% of *pas1* seedlings ($n = 74$) showed lateral root initiations in the control condition, the application of VLCFAs led to a fourfold increase in lateral root outgrowth (9% of *pas1* seedlings, $n = 88$). This result was also confirmed by the direct application of acyl-CoA to *pas1* seedlings. Whereas 16:0-CoA had no effect on the number of seedlings showing lateral root development, and 18:0-CoA had only a slight effect (13 and 20%, respectively, of seedlings compared with 10% for the control, $n = 30$), a mixture of 20:0-, 22:0-, and 24:0-CoA increased the number of seedlings initiating lateral root development (42% of seedlings, $n = 30$). The effect of VLCFA treatment on *pDR5:GFP* and *pPIN1:PIN1-GFP* distribution was also analyzed in wild-type and *pas1* roots. As for the root growth assay, the different treatment did not affect DR5 expression and PIN1-GFP localization in the wild type (data not shown). However in fatty acid-treated *pas1*, DR5 was expressed at the tips of lateral roots (Figures 4K and 4L) and PIN1-GFP was targeted to the plasma membrane (Figures 4M and 4N), demonstrating that VLCFAs are directly involved in the distribution of auxin during lateral root development.

DISCUSSION

PAS1 Is Involved in VLCFA Synthesis

Several lines of evidence suggest that altered lipid metabolism is directly involved in the *pas1* phenotype. First, *pas1*, like the *pas2* and *pas3* mutants, is characterized by lower levels of VLCFAs. Second, most of the developmental defects observed in *pas1* were also found in the *pas3* mutant, which is deficient in the synthesis of malonyl-CoA, a precursor of VLCFA synthesis (Baud et al., 2004). Third, we showed that PAS1 is localized in the ER, at the site of VLCFA synthesis and directly interacts with at least three members of the VLCFA elongase complex, KCR, ECR (CER10), and PAS2. Finally, application of exogenous VLCFAs was sufficient to rescue lateral root development in *pas1*.

VLCFAs are specific components of seed storage triacylglycerols, cuticular waxes, suberins, some phospholipids, and sphingolipids. Lack of aliphatic suberin in the root led to retarded root growth but did not change the root architecture and, in particular, lateral root development (Franke et al., 2009). Defective accumulation of VLCFAs in seed triacylglycerols or cuticle did not result in embryonic and postembryonic phenotypes equivalent to those observed in *pas1* or *pas3* mutants. However, sphingolipids are known to regulate cell polarity and differentiation (Hoekstra et al., 2003). Polarized epithelial cells showed specific sphingolipid enrichments in apical and basolateral membranes, moreover perturbing the association of polar protein with sphingolipid domains and preventing their sorting to the plasma membrane (Nyasae et al., 2003). Interestingly, sterols and sphingolipids are both involved in detergent-resistant membrane structure, and it is noteworthy that the observed GluCer reduction in *pas1* is likely associated with a compensatory increase in sterol and sterol glycoside levels (Mongrand et al., 2004; Borner et al., 2005; Laloi et al., 2007). A similar observation was described in yeast where synthetic lethality resulting from multiple mutations in the sterol biosynthetic pathway can be suppressed by mutations in the sphingolipid biosynthesis pathway (Valachovic et al., 2006). Interestingly, yeast does not seem to have a PAS1 ortholog, suggesting that the plant elongase complex, which harbors a large variety of components, such as the FAE1-like ketoacyl-CoA synthase family and ELO homologs, requires an extra enzymatic chaperone to carry out its activity.

PAS1-Dependent Synthesis of VLCFAs Is Required for Polar Auxin Distribution

In animals, part of protein sorting to apical and basolateral membranes relies on protein partitioning into sphingolipid-enriched microdomains in the trans-Golgi network and in endosomes (Hoekstra et al., 2003). Our work shows that a defect in VLCFA synthesis results in altered subcellular distribution of the polar auxin influx carrier PIN1. PIN1 polarity can be modified by several factors, including the Ser/Thr protein kinase PINOID and the lipid content of membranes. Indeed, a mutation in the *STEROL METHYL TRANSFERASE1* gene, which caused a marked decrease in sitosterol and an increase in cholesterol, leads to the redistribution of PIN1 to lateral instead of basal membranes of elongated vascular cells (Willemssen et al., 2003).

Involvement of sterols in the polar distribution of PIN proteins is supported by the fact that the PIN2 efflux carrier colocalizes with the sterol marker filipin (Grebe et al., 2003). PAS1 is thus not a general regulator of polar trafficking but instead displays some specificity toward protein cargo in the anterograde pathway, which is most likely not limited to PIN1.

Defective Auxin Distribution in *pas1* Is Associated with Abnormal Patterning during Organogenesis

Defective patterning in the apical domain of *pas1* embryos was associated with round shaped cells and random division planes, confirming that cell dedifferentiation and proliferation were associated with modified cell polarity. Alteration of cell polarity is often observed in highly proliferative cells like in mammalian cancers (Bissell and Radisky, 2001). In *Drosophila melanogaster*, loss of cell polarity is associated with Ras-induced tumor progression and invasiveness (Igaki et al., 2006). In plants, the involvement of cell polarity in cell differentiation was clearly demonstrated for polar auxin transport during organogenesis. The sequential reorientation of epidermal PIN proteins in the late globular embryo was found to be involved in the generation of

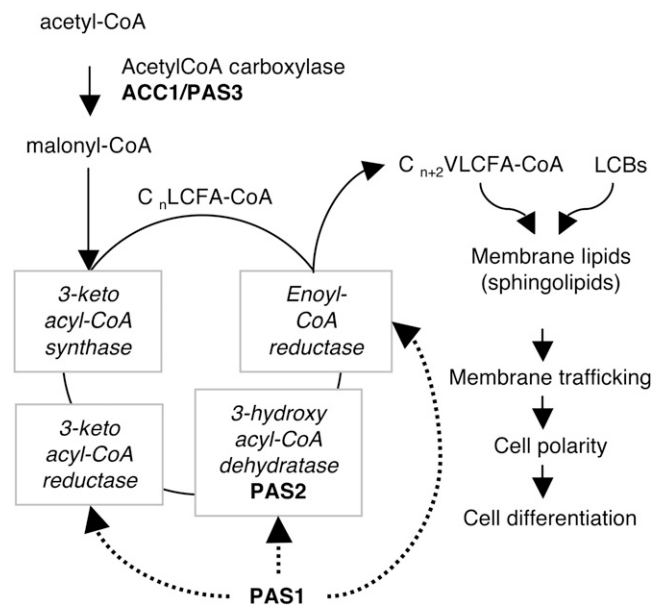


Figure 6. A Model for the Role of PAS Proteins and VLCFAs in Plant Cell Differentiation.

Fatty acid elongation requires long-chain fatty acyl-CoA (C_n LCFA-CoA) of n carbons and malonyl-CoA produced by the acetyl-CoA carboxylase PAS3. Elongation occurs in the ER membrane with four sequential reactions (boxed enzymes) to eventually produce very-long-chain fatty acyl-CoA of $n+2$ carbons (C_{n+2} VLCFA-CoA). PAS1, by its association with elongase enzymes (dashed arrows), is required for fatty acid elongation. The role of VLCFA-CoA on plant development is most probably associated with the synthesis of membrane sphingolipids with long-chain bases (LCBs). Sphingolipids have been described to be involved in membrane trafficking and cell polarity, which are key determinants of cell differentiation.

new auxin maxima at the site of cotyledon initiation (Benkova et al., 2003; Friml et al., 2003). Thus, the defective polarity of PIN1 in the apical region of *pas1-3* embryos is involved in the alteration of polar auxin transport and the lack of local redistribution of auxin accumulation. The altered auxin gradient at the embryo apex in *pas1-3* would then prevent the establishment of bilateral symmetry during embryo development as well as the formation of cotyledons. The absence of cotyledons in *pas1* would thus result from the absence of proper determination of the different apical territories that are characterized by mutually exclusive cell fates (Kajiwaru et al., 2004). Consistent with this, *PAS1* expression is enhanced in the cotyledons of late developing embryos. This result confirms the comparative transcriptome analysis of the different domains of the embryo, in which *PAS1* appears to be one of the most differentially expressed gene in the apical domains of the embryos at globular and heart stages (Casson et al., 2005). A similar association between embryo patterning and PIN1 polarity was observed for the *KANADI* gene family during the establishment of embryo bilateral symmetry (Izhaki and Bowman, 2007). Indeed, embryos of *kan1 kan2 kan4* triple mutants showed ectopic outgrowths on the hypocotyl that were caused by the reversal of PIN polarity and localized accumulation of auxin. Similarly, changes of PIN1 polarity are also known to be essential to relocate auxin into lateral root primordia. As expected, we found that the absence of lateral root development in *pas1-3* was also associated with the abnormal distribution of PIN1 but not of AUX1, demonstrating that *PAS1* regulates PIN1 polarity in specific cell types throughout plant development, from early embryonic stages to postgerminative de novo organogenesis. Interestingly, the related immunophilin TWISTED DWARF has been characterized as a regulator of auxin carrier activities of the PGP1/PGP19 ABCB transporters (Bouchard et al., 2006). Moreover, PIN1 stability at the plasma membrane is stabilized by the presence of PGP1/PGP19 (Titapiwatanakun et al., 2009). Altogether, these results support the fact that membrane-localized immunophilins are involved in the regulation of polar auxin transport.

Like many immunophilins, *PAS1* likely interacts with different substrates (Barik, 2006) and most probably acts as chaperone or scaffold factor for several ER proteins. We previously showed that *PAS1* interacts with a transcription factor of the NAC family and regulates its subcellular localization within the nucleus (Smyczynski et al., 2006). Overexpression of this transcription factor in *pas1* led to a partial rescue of the shoot apical growth (Smyczynski et al., 2006), suggesting that *PAS1* may interact with other protein substrates. Here, we showed that *PAS1* interacts with several enzymes of the elongase complex in the ER and is required for VLCFA elongation (Figure 6). Proteins of the elongase complex likely represent major *PAS1* substrates since mutations in *PAS2* and *PAS3* genes, which are directly involved in VLCFA synthesis, are epistatic to *pas1* and lead to similar developmental phenotypes (Faure et al., 1998). We showed that VLCFAs could rescue lateral root formation in *pas1*, demonstrating that *PAS1*-dependent fatty acid elongation is necessary for lateral root development. Identification of the VLCFA-derived molecules and their precise cellular functions will be essential to understand the role of lipids in the polar targeting of proteins.

METHODS

Plant Material and Growth Conditions

The *pas1-3* and *pas3-1* mutants are ethyl methanesulfonate alleles in the Columbia-0 (Col-0) background that were maintained as heterozygous stocks (Baud et al., 2003, 2004; Smyczynski et al., 2006). Lines expressing *pDR5:GFP* (Friml et al., 2003), *pPIN1:PIN1-GFP* (Benkova et al., 2003), *pCycB1;1:db-GUS*, *pWUS:GFP*, and *pAUX1:AUX1-YFP* (Swarup et al., 2001) were crossed with the *pas1-3* or *pas3-1* mutants (female donor). *PAS1* promoter sequence corresponding to the 2407-bp sequence upstream of the ATG was amplified (5'-AAAAAAGCAGGCTCCACAT-CAGGTGGATATAT-3' and 5'-AAGAAAGCTGGTCCGCCGATCAAAT-CCAGAGT-3'), cloned into pDONOR207 and recombined into pMDC162 to generate the p*PAS1*:GUS construct (Curtis and Grossniklaus, 2003). Several independent Col-0 lines expressing p*PAS1*:GUS were selected, and a representative line was selected for further studies. All the embryo analyses were performed on siliques from heterozygous *pas1-3/+* or *pas3-1/+* lines homozygous for the GFP/GUS marker construct to ensure similar developmental stages and maternal environment for wild-type and mutant embryos. Plants were grown in the greenhouse in soil (Tref Substrates) and watered with Plant-Prod nutritive solution (Fertil). Seedlings were germinated on *Arabidopsis thaliana* agar medium (Estelle and Somerville, 1987) and grown for 10 d under constant temperature 18°C, 16-h/8-h light/dark cycle, and with 60% humidity. VLCFA complementation was performed by germinating seedlings on horizontal *Arabidopsis* medium plates then transferring them to a vertical position for 10 d. Seedlings were then transferred to horizontal plates supplemented with 200 μ M free fatty acids for 4 to 6 d. Free fatty acids and acyl-CoA (18:0, 20:0, 22:0, and 24:0) were prepared as 20 mM stock solutions in toluene and DMSO, respectively. Control experiments were performed with toluene or DMSO supplemented plates.

Cytological Analyses

Embryos were fixed, stained with propidium iodide, and finally cleared with chloral hydrate (Truernit et al., 2008). In situ hybridizations were performed on serial sections of siliques at different stages as described previously (Vernoux et al., 2000; Nikovics et al., 2006). For immunolocalization, samples were fixed for 1 h in 4% (w/v) paraformaldehyde, embedded in paraplast, and sectioned as previously described (Smyczynski et al., 2006). Epitope demasking was performed by incubating the slides in 10 mM citrate buffer, pH 6, in a microwave oven until boiling and then washing in PBS. Samples were then incubated for 2 h at 37°C in primary antibody diluted 1/250 in PBS containing 2% (w/v) BSA, washed with PBS (three changes, 3 min per wash), and then incubated for 2 h at 37°C in secondary antibody, goat anti-rabbit-IgG antibody conjugated to Alexa Fluor 488 (Molecular Probes, Invitrogen), diluted 1:500 in PBS. After washing in PBS (three changes, 3 min per wash), the samples were mounted in antifading agent (Citifluor; Oxford Instruments). PIN1 was probed with an anti-PIN1 polyclonal serum described previously (Boutte et al., 2006).

Observations were performed using an inverted Leica TCS SP2-AOBS spectral confocal laser microscope (Leica Microsystems) using either a PL APO 20X0.70 NA or 63X1.20 NA water immersion objective. GFP and Alexa 488 fluorescence were recorded after an excitation at 488 nm (argon laser) and a selective emission band of 505 to 525 nm. Propidium iodide fluorescence was recorded with an excitation at 488 nm and emission band of 600 to 700 nm. GUS staining was performed as described previously (Harrar et al., 2003). BiFC experiments were performed as described earlier (Marion et al., 2008). *PAS2*, *KCR*, *CER10*, and *DPL1* BiFC constructs were described by Bach et al. (2008), and *SBH2* cloning was reported previously (Chen et al., 2008; Marion et al., 2008). *PAS1*

coding sequence was amplified (5'-AAAAAGCAGGCTTCATGGCGG-TAGGCGATCAGACG-3' and 5'-CAAGAAAGCTGGGTCTGTAATTTG-GCGCTCACAAA-3') and cloned in pDONOR207. Briefly, all the different open reading frames were cloned from pDONOR207 by GATEWAY recombination (Invitrogen) in pBIFC vectors in both N and C configuration with either N-ter YFP or C-ter YFP and under the control of the 35S promoter (Desprez et al., 2007; Marion et al., 2008). The four different constructs expressed under the control of the 35S promoter were systematically tested leading to eight interaction assays per pair of proteins. The ER marker CD3-959:mCherry was used as previously described (Marion et al., 2008).

BFA sensitivity was measured on 7-d-old seedlings (pPIN1:PIN1-GFP in Col-0 or in *pas1-3* background) grown on *Arabidopsis* agar medium and treated with 10, 17.8, 25, 50, or 100 μ M BFA for 30 min. Seedlings were mounted in the BFA solution, and GFP fluorescence was recorded for 30 min. Percentages of cells carrying BFA compartments were estimated in an average of 25 roots (700 cells, three replicates) per treatment.

Lipid Analyses

Mass Quantification of Lipid Species

Triacylglycerol analysis was performed as previously described (Bach et al., 2008). GIPC, GluCer, and Cer from *Arabidopsis* wild-type and mutant seedlings were extracted, isolated, and quantified as detailed by Markham and Jaworski (2007). Long-chain bases of sphingolipids (LCB) were determined as previously described by Borner et al. (2005). To isolate neutral lipids, total lipids were loaded onto HPTLC plates developed in hexane/ethylether/acetic acid (90:15:2, v/v) and separated into diacylglycerols (R_F 0.08), sterols (R_F 0.17), fatty alcohols (R_F 0.22), and free fatty acids (R_F 0.29). Lipids were identified by comigration with known standards and quantified by densitometry analysis (Macala et al., 1983) using a TLC scanner 3 (CAMAG).

De Novo Synthesis of Ceramides and Glucosylceramides

Arabidopsis wild-type and mutant seedlings were placed in small tubes and incubated with 10 μ Ci of [14 C]acetate (54 Ci/mol) in 1 mL of distilled water at 24°C for 0 to 240 min. After incubations, seedlings were washed with distilled water three times to recover the remaining acetate. Lipids were extracted by chloroform:methanol (2:1, v/v) for 60 min at 60 to 70°C and then washed three times with 9% NaCl. The solvent was evaporated and lipids were dissolved in an appropriate volume of chloroform/methanol (1:1, v/v). Polar lipids were analyzed by loading total lipids onto HPTLC plates (60F254; Merck), which were developed in methyl acetate/*n*-propanol/chloroform/methanol/0.25% aqueous KCl (25:25:25:10:9, v/v) (Heape et al., 1985). Under such conditions, glucosylceramides and sterol-glycosides were not separated. To allow their separation, the corresponding spot was further applied onto an HPTLC plate developed with chloroform/methanol (85:15, v/v) (Hillig et al., 2003). Ceramides were isolated on HPTLC plates as described previously (Heape et al., 1995). Labeling of the different lipids was determined and quantified with a phosphor imager (Molecular Dynamics).

Accession Numbers

Sequence data from this article can be found in the Arabidopsis Genome Initiative or GenBank/EMBL databases under the following accession numbers: PAS1, At3g54010; PAS2, At5g10480; PAS3, At1g36160; DPL1, At1g27980; KCR, At1g67730; CER10, At3g55360; SBH2, At1g14290; PIN1, At1g73590; AUX1, At2g38120; WUS, At2g17950; and ANT, At4g37750.

Supplemental Data

The following materials are available in the online version of this article.

Supplemental Figure 1. VLCFA and Sphingolipid Biosynthesis Is Altered in *pas1-3* and *pas3-1* Mutants.

Supplemental Figure 2. Ceramide, Hydroxyceramide, Glucosylceramide, and Glycosylinositolphosphorylceramide Composition of *pas1-3* and *pas3-1* Mutants.

Supplemental Figure 3. PAS1 Interacts with Elongase Enzymes.

Supplemental Figure 4. Morphology of *pas1-3* Embryos at Late Torpedo Stage.

Supplemental Figure 5. The Cell Division Pattern Is Not Modified in the *pas1-3* Mutant.

Supplemental Figure 6. The WUS Domain Is Larger in *pas1-3*.

Supplemental Figure 7. Altered PIN1 Distribution in *pas1-3/+* Embryos at Late Globular to Early Heart Stage.

Supplemental Figure 8. Auxin Accumulation and PIN1 Polar Distribution Are Altered in *pas3* Embryo.

Supplemental Figure 9. PAS1 Is Involved in Lateral Root Development.

Supplemental Figure 10. Polar Auxin Transport during *pas1* Root Development.

Supplemental Figure 11. *pDR5:GFP* Expression in Emerging Lateral Roots of Wild-Type Seedlings.

Supplemental Table 1. Relative Sterol and Sterol Glycoside Levels in *pas1* and *pas3* Mutants.

ACKNOWLEDGMENTS

F.R. was funded by a "Haigneré" Institut National de la Recherche Agronomique postdoctoral fellowship. A.L. was funded by the European Union Marie Curie short-stay training program (Versailles-Evry Research Training program). J.M. and C.R. were funded by the 6th European Integrated Project AGRON-OMICS (Grant LSHG-CT-2006-037704). L.B. was funded by the Bourses Cancéropôle Ile-de-France. D.M. was funded by the European Union Versailles-Evry Research Training program and Agence Nationale pour la Recherche (07-BLAN-202). We thank Jan Traas (Ecole Normale Supérieure, Lyon), Malcolm Bennett (University of Nottingham), Patrick Laufs (Institut National de la Recherche Agronomique, Versailles) for the gifts of pPIN1-PIN1:GFP, pAUX1-AUX1:YFP, and pWUS:GFP constructs, respectively. We thank Olivier Grandjean and the Plateforme Cytologie et d'Imagerie du Végétal de Versailles for their great help in confocal microscopy as well as Bruno Letarnec for taking care of the plants. The work was partially funded by the ANR blanc SphingopolaR (ANR-07-BLAN-0202). Rothamsted Research receives grant-aided support from the Biotechnology and Biological Sciences Research Council.

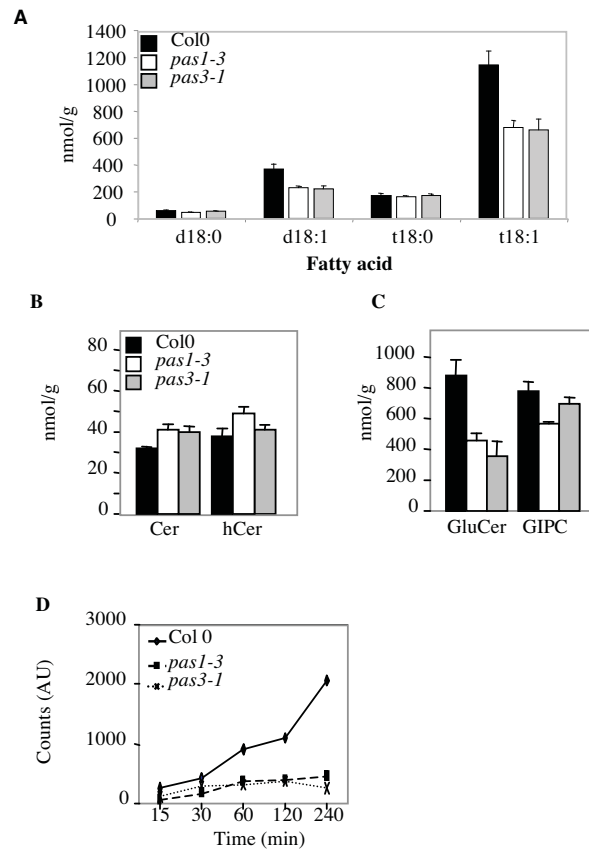
Received September 8, 2009; revised January 21, 2010; accepted January 27, 2010; published February 9, 2010.

REFERENCES

- Aida, M., Vernoux, T., Furutani, M., Traas, J., and Tasaka, M.** (2002). Roles of PIN-FORMED1 and MONOPTEROS in pattern formation of the apical region of the Arabidopsis embryo. *Development* **129**: 3965–3974.
- Bach, L., et al.** (2008). The plant very long chain hydroxy fatty Acyl-CoA dehydratase PASTICCINO2 is essential and limiting for plant development. *Proc. Natl. Acad. Sci. USA* **105**: 14727–14731.
- Barik, S.** (2006). Immunophilins: for the love of proteins. *Cell. Mol. Life Sci.* **63**: 2889–2900.

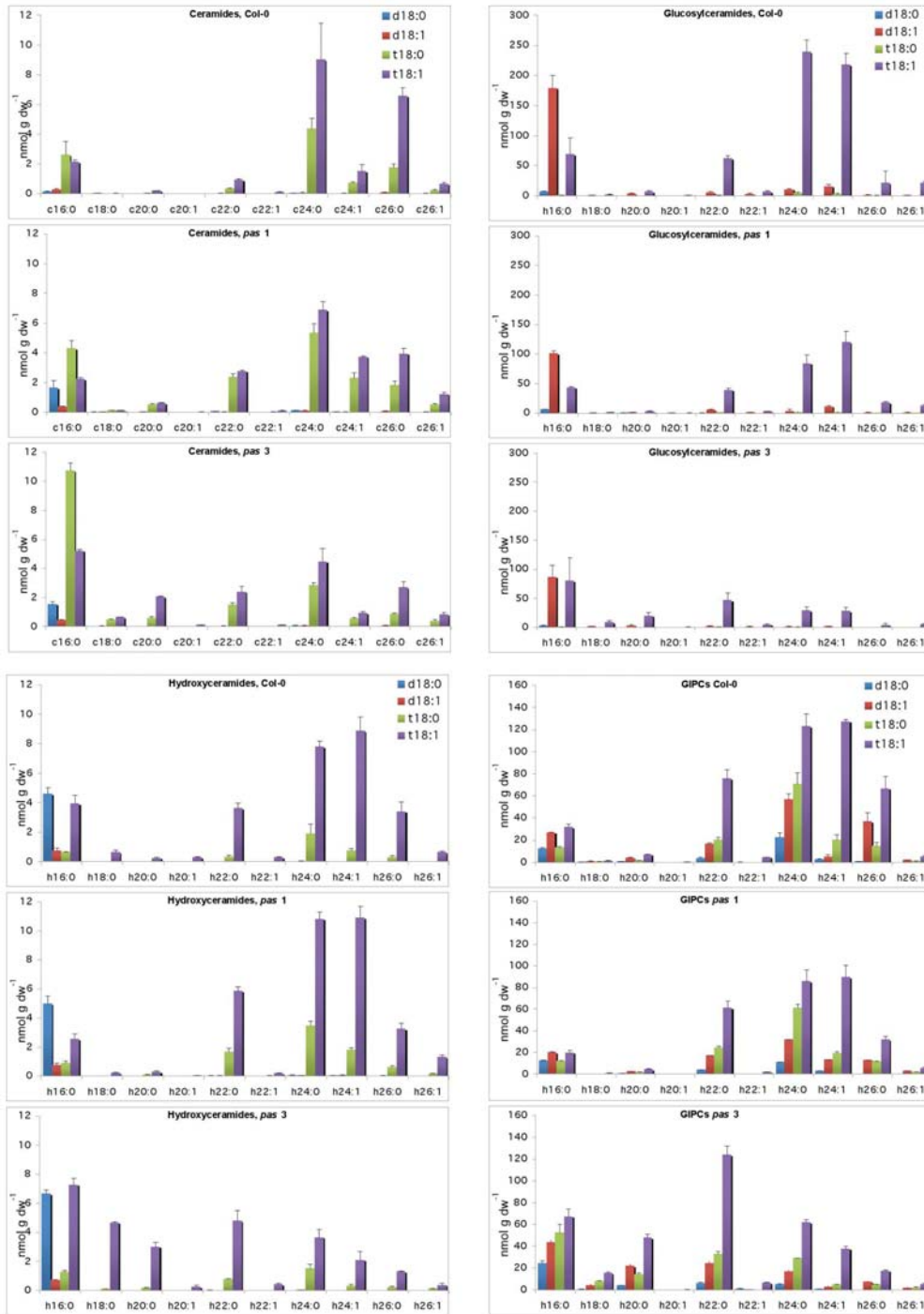
- Baud, S., Bellec, Y., Miquel, M., Bellini, C., Caboche, M., Lepiniec, L., Faure, J.D., and Rochat, C.** (2004). *gurke* and *pasticcino3* mutants affected in embryo development are impaired in acetyl-CoA carboxylase. *EMBO Rep.* **5**: 1–6.
- Baud, S., Guyon, V., Kronenberger, J., Wuillème, S., Miquel, M., Caboche, M., Lepiniec, L., and Rochat, C.** (2003). Multifunctional acetyl-CoA carboxylase 1 is essential for very long chain fatty acids elongation and embryo development in *Arabidopsis*. *Plant J.* **33**: 75–86.
- Beaudoin, F., Wu, X., Li, F., Haslam, R.P., Markham, J.E., Zheng, H., Napier, J.A., and Kunst, L.** (2009). Functional characterization of the *Arabidopsis* beta-ketoacyl-coenzyme A reductase candidates of the fatty acid elongase. *Plant Physiol.* **150**: 1174–1191.
- Benkova, E., Michniewicz, M., Sauer, M., Teichmann, T., Seifertova, D., Jurgens, G., and Friml, J.** (2003). Local, efflux-dependent auxin gradients as a common module for plant organ formation. *Cell* **115**: 591–602.
- Bissell, M.J., and Radisky, D.** (2001). Putting tumours in context. *Nat. Rev. Cancer* **1**: 46–54.
- Borner, G.H., Sherrier, D.J., Weimar, T., Michaelson, L.V., Hawkins, N.D., Macaskill, A., Napier, J.A., Beale, M.H., Lilley, K.S., and Dupree, P.** (2005). Analysis of detergent-resistant membranes in *Arabidopsis*. Evidence for plasma membrane lipid rafts. *Plant Physiol.* **137**: 104–116.
- Bouchard, R., Bailly, A., Blakeslee, J.J., Oehring, S.C., Vincenzetti, V., Lee, O.R., Paponov, I., Palme, K., Mancuso, S., Murphy, A.S., Schulz, B., and Geisler, M.** (2006). Immunophilin-like TWISTED DWARF1 modulates auxin efflux activities of *Arabidopsis* P-glycoproteins. *J. Biol. Chem.* **281**: 30603–30612.
- Boutte, Y., Crosnier, M.T., Carraro, N., Traas, J., and Satiat-Jeuemaitre, B.** (2006). The plasma membrane recycling pathway and cell polarity in plants: studies on PIN proteins. *J. Cell Sci.* **119**: 1255–1265.
- Casson, S., Spencer, M., Walker, K., and Lindsey, K.** (2005). Laser capture microdissection for the analysis of gene expression during embryogenesis of *Arabidopsis*. *Plant J.* **42**: 111–123.
- Chen, M., Han, G., Dietrich, C.R., Dunn, T.M., and Cahoon, E.B.** (2006). The essential nature of sphingolipids in plants as revealed by the functional identification and characterization of the *Arabidopsis* LCB1 subunit of serine palmitoyltransferase. *Plant Cell* **18**: 3576–3593.
- Chen, M., Markham, J.E., Dietrich, C.R., Jaworski, J.G., and Cahoon, E.B.** (2008). Sphingolipid long-chain base hydroxylation is important for growth and regulation of sphingolipid content and composition in *Arabidopsis*. *Plant Cell* **20**: 1862–1878.
- Colon-Carmona, A., You, R., Haimovitch-Gal, T., and Doerner, P.** (1999). Technical advance: Spatio-temporal analysis of mitotic activity with a labile cyclin-GUS fusion protein. *Plant J.* **20**: 503–508.
- Curtis, M.D., and Grossniklaus, U.** (2003). A gateway cloning vector set for high-throughput functional analysis of genes in plants. *Plant Physiol.* **133**: 462–469.
- Da Costa, M., Bach, L., Landrieu, I., Bellec, Y., Catrice, O., Brown, S., De Veylder, L., Lippens, G., Inze, D., and Faure, J.D.** (2006). *Arabidopsis* PASTICCINO2 is an antiphosphatase involved in regulation of cyclin-dependent kinase A. *Plant Cell* **18**: 1426–1437.
- Desprez, T., Juraniec, M., Crowell, E.F., Jouy, H., Pochylova, Z., Parcy, F., Hofte, H., Gonneau, M., and Vernhettes, S.** (2007). Organization of cellulose synthase complexes involved in primary cell wall synthesis in *Arabidopsis thaliana*. *Proc. Natl. Acad. Sci. USA* **104**: 15572–15577.
- Dunn, T.M., Lynch, D.V., Michaelson, L.V., and Napier, J.A.** (2004). A post-genomic approach to understanding sphingolipid metabolism in *Arabidopsis thaliana*. *Ann. Bot. (Lond.)* **93**: 483–497.
- Estelle, M., and Somerville, C.** (1987). Auxin-resistant mutants of *Arabidopsis thaliana* with an altered morphology. *Mol. Gen. Genet.* **206**: 200–206.
- Faure, J.D., Vittorioso, P., Santoni, V., Frasier, V., Prinsen, E., Barlier, I., Vanonckelen, H., Caboche, M., and Bellini, C.** (1998). The PASTICCINO genes of *Arabidopsis thaliana* are involved in the control of cell division and differentiation. *Development* **125**: 909–918.
- Franke, R., Hofer, R., Briesen, I., Emsermann, M., Efremova, N., Yephremov, A., and Schreiber, L.** (2009). The DAISY gene from *Arabidopsis* encodes a fatty acid elongase condensing enzyme involved in the biosynthesis of aliphatic suberin in roots and the chalaza-micropyle region of seeds. *Plant J.* **57**: 80–95.
- Friml, J., Vieten, A., Sauer, M., Weijers, D., Schwarz, H., Hamann, T., Offringa, R., and Jurgens, G.** (2003). Efflux-dependent auxin gradients establish the apical-basal axis of *Arabidopsis*. *Nature* **426**: 147–153.
- Fu, A., He, Z., Cho, H.S., Lima, A., Buchanan, B.B., and Luan, S.** (2007). A chloroplast cyclophilin functions in the assembly and maintenance of photosystem II in *Arabidopsis thaliana*. *Proc. Natl. Acad. Sci. USA* **104**: 15947–15952.
- Furutani, M., Vernoux, T., Traas, J., Kato, T., Tasaka, M., and Aida, M.** (2004). PIN-FORMED1 and PINOID regulate boundary formation and cotyledon development in *Arabidopsis* embryogenesis. *Development* **131**: 5021–5030.
- Geldner, N., Anders, N., Wolters, H., Keicher, J., Kornberger, W., Muller, P., Delbarre, A., Ueda, T., Nakano, A., and Jurgens, G.** (2003). The *Arabidopsis* GNOM ARF-GEF mediates endosomal recycling, auxin transport, and auxin-dependent plant growth. *Cell* **112**: 219–230.
- Geldner, N., Friml, J., Stierhof, Y.D., Jurgens, G., and Palme, K.** (2001). Auxin transport inhibitors block PIN1 cycling and vesicle trafficking. *Nature* **413**: 425–428.
- Grebe, M., Xu, J., Mobius, W., Ueda, T., Nakano, A., Geuze, H.J., Rook, M.B., and Scheres, B.** (2003). *Arabidopsis* sterol endocytosis involves actin-mediated trafficking via ARA6-positive early endosomes. *Curr. Biol.* **13**: 1378–1387.
- Haberer, G., Erschadi, S., and Torres-Ruiz, R.A.** (2002). The *Arabidopsis* gene PEPINO/PASTICCINO2 is required for proliferation control of meristematic and non-meristematic cells and encodes a putative anti-phosphatase. *Dev. Genes Evol.* **212**: 542–550.
- Harrar, Y., Bellec, Y., Bellini, C., and Faure, J.D.** (2003). Hormonal control of cell proliferation requires PASTICCINO genes. *Plant Physiol.* **132**: 1217–1227.
- Harrar, Y., Bellini, C., and Faure, J.D.** (2001). FKBP: At the crossroads of folding and transduction. *Trends Plant Sci.* **6**: 426–431.
- Heape, A.M., Bessoule, J.J., Boiron-Sargueil, F., Garbay, B., and Cassagne, C.** (1995). Sphingolipid metabolic disorders in Trembler mouse peripheral nerves in vivo result from an abnormal substrate supply. *J. Neurochem.* **65**: 1665–1673.
- Heape, A.M., Juguelin, H., Boiron, F., and Cassagne, C.** (1985). Improved one-dimensional thin-layer chromatographic technique for polar lipids. *J. Chromatogr. A* **322**: 391–395.
- Hillig, I., Leipelt, M., Ott, C., Zahringer, U., Warnecke, D., and Heinz, E.** (2003). Formation of glucosylceramide and sterol glucoside by a UDP-glucose-dependent glucosylceramide synthase from cotton expressed in *Pichia pastoris*. *FEBS Lett.* **553**: 365–369.
- Hoekstra, D., Maier, O., van der Wouden, J.M., Slimane, T.A., and van IJzendoorn, S.C.** (2003). Membrane dynamics and cell polarity: The role of sphingolipids. *J. Lipid Res.* **44**: 869–877.
- Igaki, T., Pagliarini, R.A., and Xu, T.** (2006). Loss of cell polarity drives tumor growth and invasion through JNK activation in *Drosophila*. *Curr. Biol.* **16**: 1139–1146.
- Izhaki, A., and Bowman, J.L.** (2007). KANADI and class III HD-Zip gene families regulate embryo patterning and modulate auxin flow during embryogenesis in *Arabidopsis*. *Plant Cell* **19**: 495–508.
- Jaillais, Y., Fobis-Loisy, I., Miede, C., Rollin, C., and Gaude, T.** (2006).

- AtSNX1 defines an endosome for auxin-carrier trafficking in *Arabidopsis*. *Nature* **443**: 106–109.
- Jenik, P.D., and Barton, M.K. (2005). Surge and destroy: The role of auxin in plant embryogenesis. *Development* **132**: 3577–3585.
- Joubes, J., Raffaele, S., Bourdenx, B., Garcia, C., Laroche-Traineau, J., Moreau, P., Domergue, F., and Lessire, R. (2008). The VLCFA elongase gene family in *Arabidopsis thaliana*: Phylogenetic analysis, 3D modelling and expression profiling. *Plant Mol. Biol.* **67**: 547–566.
- Kajiwara, T., Furutani, M., Hibara, K., and Tasaka, M. (2004). The GURKE gene encoding an acetyl-CoA carboxylase is required for partitioning the embryo apex into three subregions in *Arabidopsis*. *Plant Cell Physiol.* **45**: 1122–1128.
- Laloi, M., et al. (2007). Insights into the role of specific lipids in the formation and delivery of lipid microdomains to the plasma membrane of plant cells. *Plant Physiol.* **143**: 461–472.
- Macala, L.J., Yu, R.K., and Ando, S. (1983). Analysis of brain lipids by high performance thin-layer chromatography and densitometry. *J Lipid Res.* **24**: 1243–1250.
- Marion, J., Bach, L., Bellec, Y., Meyer, C., Gissot, L., and Faure, J.D. (2008). Systematic analysis of protein subcellular localization and interaction using high-throughput transient transformation of *Arabidopsis* seedlings. *Plant J.* **56**: 169–179.
- Markham, J.E., and Jaworski, J.G. (2007). Rapid measurement of sphingolipids from *Arabidopsis thaliana* by reversed-phase high-performance liquid chromatography coupled to electrospray ionization tandem mass spectrometry. *Rapid Commun. Mass Spectrom.* **21**: 1304–1314.
- Markham, J.E., Li, J., Cahoon, E.B., and Jaworski, J.G. (2006). Plant sphingolipids: Separation and identification of major sphingolipid classes from leaves. *J. Biol. Chem.* **281**: 22684–22694.
- Millar, A.A., and Kunst, L. (1997). Very-long-chain fatty acid biosynthesis is controlled through the expression and specificity of the condensing enzyme. *Plant J.* **12**: 121–131.
- Mongrand, S., Morel, J., Laroche, J., Claverol, S., Carde, J.P., Hartmann, M.A., Bonneu, M., Simon-Plas, F., Lessire, R., and Bessoule, J.J. (2004). Lipid rafts in higher plant cells: Purification and characterization of Triton X-100-insoluble microdomains from tobacco plasma membrane. *J. Biol. Chem.* **279**: 36277–36286.
- Muday, G.K., Peer, W.A., and Murphy, A.S. (2003). Vesicular cycling mechanisms that control auxin transport polarity. *Trends Plant Sci.* **8**: 301–304.
- Nikovics, K., Blein, T., Peaucelle, A., Ishida, T., Morin, H., Aida, M., and Laufs, P. (2006). The balance between the MIR164A and CUC2 genes controls leaf margin serration in *Arabidopsis*. *Plant Cell* **18**: 2929–2945.
- Nyasae, L.K., Hubbard, A.L., and Tuma, P.L. (2003). Transcytotic efflux from early endosomes is dependent on cholesterol and glycosphingolipids in polarized hepatic cells. *Mol. Biol. Cell* **14**: 2689–2705.
- Reina-Pinto, J.J., Voisin, D., Kurdyukov, S., Faust, A., Haslam, R.P., Michaelson, L.V., Efremova, N., Franke, B., Schreiber, L., Napier, J.A., and Yephremov, A. (2009). Misexpression of FATTY ACID ELONGATION1 in the *Arabidopsis* epidermis induces cell death and suggests a critical role for phospholipase A2 in this process. *Plant Cell* **21**: 1252–1272.
- Schaller, H. (2004). New aspects of sterol biosynthesis in growth and development of higher plants. *Plant Physiol. Biochem.* **42**: 465–476.
- Smyczynski, C., Roudier, F., Gissot, L., Vaillant, E., Grandjean, O., Morin, H., Masson, T., Bellec, Y., Geelen, D., and Faure, J.D. (2006). The C terminus of the immunophilin PASTICCINO1 is required for plant development and for interaction with a NAC-like transcription factor. *J. Biol. Chem.* **281**: 25475–25484.
- Steinmann, T., Geldner, N., Grebe, M., Mangold, S., Jackson, C.L., Paris, S., Galweiler, L., Palme, K., and Jurgens, G. (1999). Coordinated polar localization of auxin efflux carrier PIN1 by GNOM ARF GEF. *Science* **286**: 316–318.
- Swarup, R., Friml, J., Marchant, A., Ljung, K., Sandberg, G., Palme, K., and Bennett, M. (2001). Localization of the auxin permease AUX1 suggests two functionally distinct hormone transport pathways operate in the *Arabidopsis* root apex. *Genes Dev.* **15**: 2648–2653.
- Tanaka, H., Dhonukshe, P., Brewer, P.B., and Friml, J. (2006). Spatiotemporal asymmetric auxin distribution: A means to coordinate plant development. *Cell. Mol. Life Sci.* **63**: 2738–2754.
- Titapiwatanakun, B., et al. (2009). ABCB19/PGP19 stabilises PIN1 in membrane microdomains in *Arabidopsis*. *Plant J.* **57**: 27–44.
- Tremli, B.S., Winderl, S., Radykewicz, R., Herz, M., Schweizer, G., Hutzler, P., Glawischnig, E., and Ruiz, R.A. (2005). The gene ENHANCER OF PINOID controls cotyledon development in the *Arabidopsis* embryo. *Development* **132**: 4063–4074.
- Truernit, E., Bauby, H., Dubreucq, B., Grandjean, O., Runions, J., Barthelemy, J., and Palauqui, J.C. (2008). High-resolution whole-mount imaging of three-dimensional tissue organization and gene expression enables the study of phloem development and structure in *Arabidopsis*. *Plant Cell* **20**: 1494–1503.
- Tsegaye, Y., Richardson, C.G., Bravo, J.E., Mulcahy, B.J., Lynch, D. V., Markham, J.E., Jaworski, J.G., Chen, M., Cahoon, E.B., and Dunn, T.M. (2007). *Arabidopsis* mutants lacking long chain base phosphate lyase are fumonisin-sensitive and accumulate trihydroxy-18:1 long chain base phosphate. *J. Biol. Chem.* **282**: 28195–28206.
- Valachovic, M., Bareither, B.M., Shah Alam Bhuiyan, M., Eckstein, J., Barbuch, R., Balderes, D., Wilcox, L., Sturley, S.L., Dickson, R. C., and Bard, M. (2006). Cumulative mutations affecting sterol biosynthesis in the yeast *Saccharomyces cerevisiae* result in synthetic lethality that is suppressed by alterations in sphingolipid profiles. *Genetics* **173**: 1893–1908.
- Vernoux, T., Kronenberger, J., Grandjean, O., Laufs, P., and Traas, J. (2000). PIN-FORMED 1 regulates cell fate at the periphery of the shoot apical meristem. *Development* **127**: 5157–5165.
- Vittorioso, P., Cowling, R., Faure, J.D., Caboche, M., and Bellini, C. (1998). Mutation in the *Arabidopsis* PASTICCINO1 gene, which encodes a new FK506-binding protein-like protein, has a dramatic effect on plant development. *Mol. Cell. Biol.* **18**: 3034–3043.
- Willemsen, V., Friml, J., Grebe, M., van den Toorn, A., Palme, K., and Scheres, B. (2003). Cell polarity and PIN protein positioning in *Arabidopsis* require STEROL METHYLTRANSFERASE1 function. *Plant Cell* **15**: 612–625.
- Zheng, H., Rowland, O., and Kunst, L. (2005). Disruptions of the *Arabidopsis* Enoyl-CoA reductase gene reveal an essential role for very-long-chain fatty acid synthesis in cell expansion during plant morphogenesis. *Plant Cell* **17**: 1467–1481.

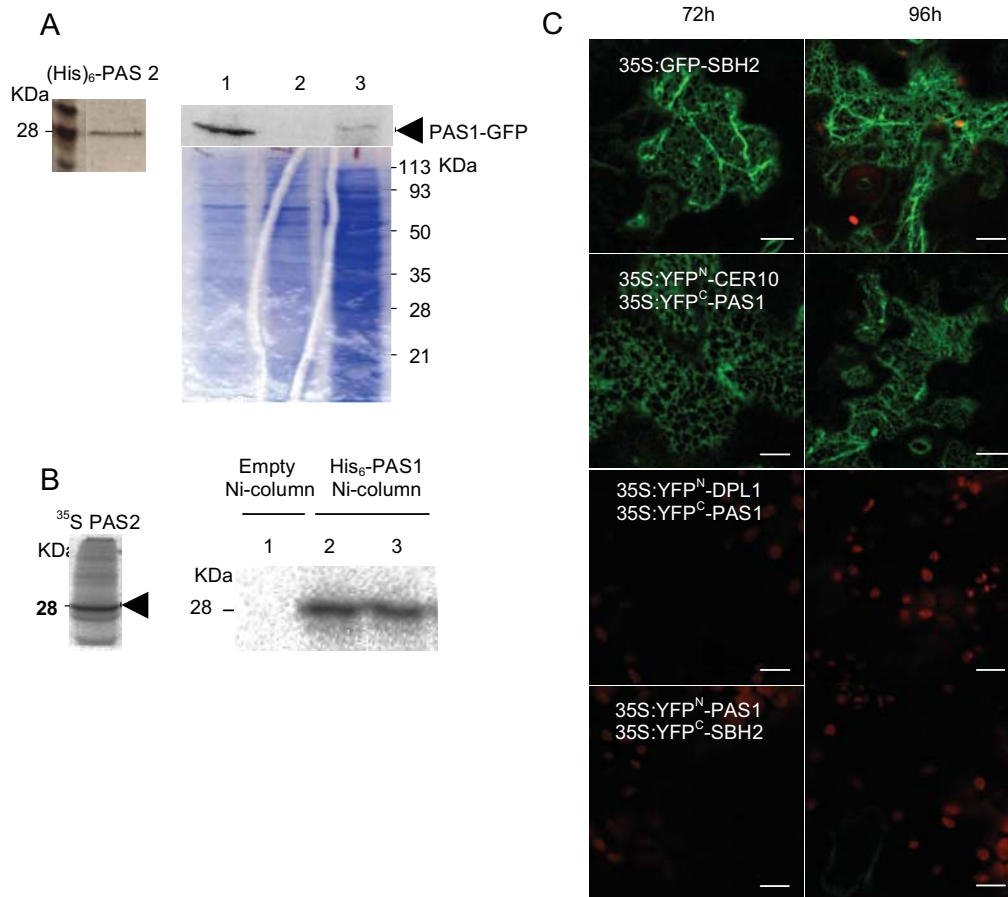


Supplemental Figure 1 . VLCFAs and sphingolipids biosynthesis are altered in *pas1-3* and *pas3-1* mutants.

- (A) Long Chain base composition in total sphingolipids of *pas1-3* and *pas3-1* mutants.
- (B - C) Ceramides (Cer), hydroxyceramides (hCer) (A) and Glucosylceramides (GluCer), Glycosylinositolphosphoceramides (GIPC) (B) composition in wild-type (Col0, black bars), *pas1-3* (white bars) and *pas3-1* (grey bars) seedlings.
- (D) GluCer synthesis in wild-type (Col0), *pas1-3* and *pas3-1* mutants. Glucer synthesis was analyzed after ^{14}C -acetate pulse labeling during the time indicated.
- Data represents the mean of 3 independent analyses except for (D) where a representative experiment is shown. Error bar is SEM.



Supplemental Figure 2. Ceramides, hydroxyceramides, Glucosylceramides and Glycosylinositolphosphorylceramides (GIPCs) composition of *pas1-3* (*pas1*) and *pas3-1* (*pas3*) mutants. The level of each sphingolipid was analyzed from wild-type, *pas1-3* and *pas3-1* seedlings and separated according to their fatty acyl length (labelled c for ceramides and h for hydroxyceramides, Glucer and GIPC since they are hydroxylated) and the nature of the Long Chain Base (LCB) moiety (d18:0, d18:1, t18:0, t18:1). Results are the mean of three independent experiments; error bar is SEM.

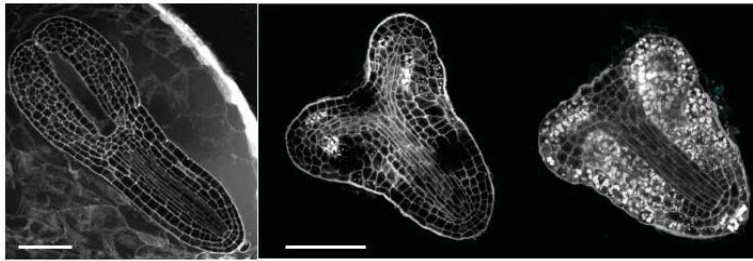


Supplemental Figure 3: PAS1 interacts with elongase enzymes.

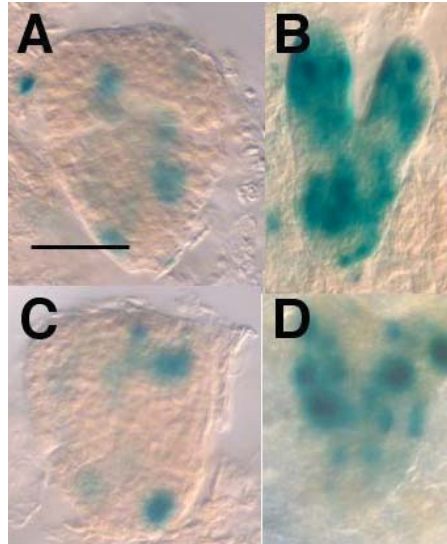
(A) The histidine tagged PAS2 protein (His₆-PAS2) was produced in the Rapid Translation System cell free system (RTS, Roche Inc). Expression of tagged PAS2 protein was monitored by silver staining of a SDS-PAGE (left) and used to prepare an affinity Ni-based affinity column (His₆-PAS2). Total extract was prepared from several grams of cells that were ground in liquid nitrogen and 1–4 mg/ml protein was extracted in extraction buffer (60 mM Tris, pH 6.8, 20% glycerol, 10 mM dithiothreitol, 0.1% Triton, and protease inhibitors). Protein extract from BY2 cells expressing 35S: PAS1-GFP (3) was used to load a Ni PAS2 column (1), or an empty Ni column (2). After washing, proteins were eluted and analyzed by western blot with an anti GFP antibody (Roche Applied Science) (right top). Proteins from the eluates of both columns (1 and 2) as well as total extract (3) were also coomassie stained (right below). The transgenic BY2 cell line expressing 35S: PAS1-GFP was described previously (Smoczynski et al. 2006). The *in vitro* pull-down using recombinant Ni-PAS2 affinity column was performed according to Da Costa et al. 2006.

(B) Radiolabelled PAS2 was produced in RTS like in (A) except that synthesis was performed in presence of ³⁵S-methionine. ³⁵S-PAS2 synthesis was monitored by autoradiography of a SDS-PAGE (left). ³⁵S-PAS2 was loaded on an empty Ni-Column (1) or two independent His₆-PAS1 Ni-columns (2, 3). The *in vitro* pull-down was performed like in (A).

(C) PAS1 interacts specifically with CER10 72 (left) and 96h (right) after transformation. Expression of 35S:GFP-SBH2, 35S:YFP^N-CER10/35S:YFP^C-PAS1, 35S:YFP^N-PAS1/35S:DPL1-YFP^C, 35SYFP^N-PAS1/35S:YFP^C-SBH2 in Arabidopsis epidermal cotyledon cells. Red signal is the plastid autofluorescence. Bars are 10 μm.

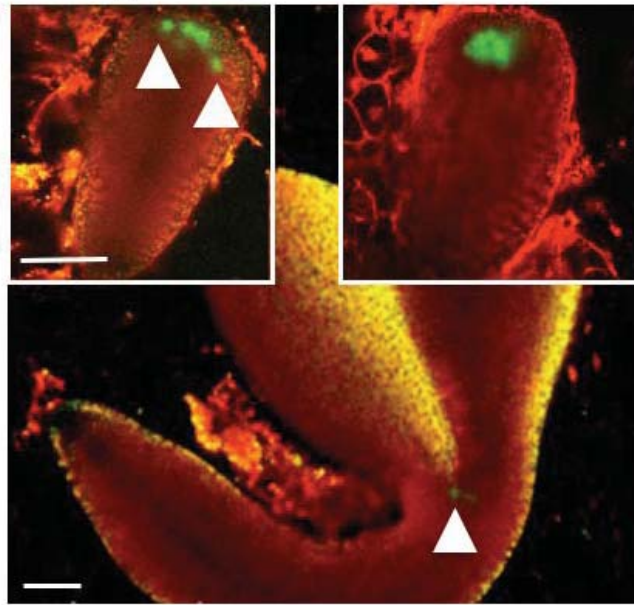


Supplemental Figure 4. Morphology of *pas1-3* embryos at late torpedo stage showing intermediate phenotype with the development of cotyledon structures, which will never expand (middle and right). Wild-type embryo from *pas1/+* silique at the same stage is shown left. Starch could be observed as white dense cellular material stained with propidium iodide. Note starch staining in *pas1-3* cotyledon (arrow head). Bar, 40 μ m

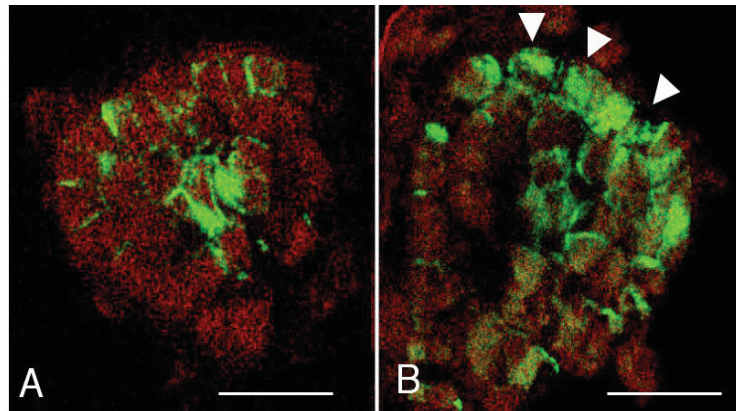


Supplemental Figure 5. Cell division pattern is not modified in *pas1-3* mutant.

Expression of the mitotic marker *pCycB1;1:db-GUS* was monitored in wild-type (A-B) and *pas1-3* (C-D) embryos. The *pCycB1;1:db-GUS* expression was analyzed at two different developmental stages: heart (A and C) and torpedo (B-D) stages. *pas1-3* and wild-type embryos were isolated from the same *pas1-3/+* silique. Bar, 40 μm

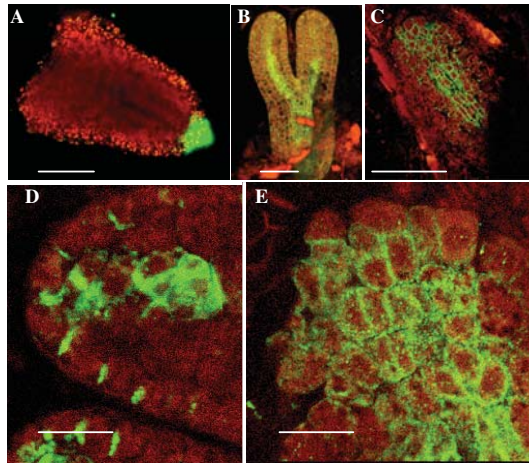


Supplemental Figure 6. The *WUS* domain is larger in *pas1-3*.
pWUS:GFP expression was monitored in wild-type (bottom) and mutant (top) embryos. *WUS* expression domain is enlarged and scattered in several non-adjacent cells (arrows) in *pas1-3* embryos as opposed to wild-type (arrows). The embryos are at the same developmental stage. Bar, 40 μ m



Supplemental Figure 7. Altered PIN1 distribution in *pas1-3/+* embryos at late globular - early heart stage.

PIN1 immunolocalization was performed on late globular embryos from segregating *pas1/+* siliques. At this stage, wild-type and *pas1-3* embryos do not show a significant phenotypic difference but segregating embryos based on their PIN1 distribution in apical cells could be observed. Some embryos showed clear aggregation and unpolar distribution of PIN1 (B, arrows) while the majority of the embryos showed polar distribution of PIN1 (A). Bar, 10 μm .

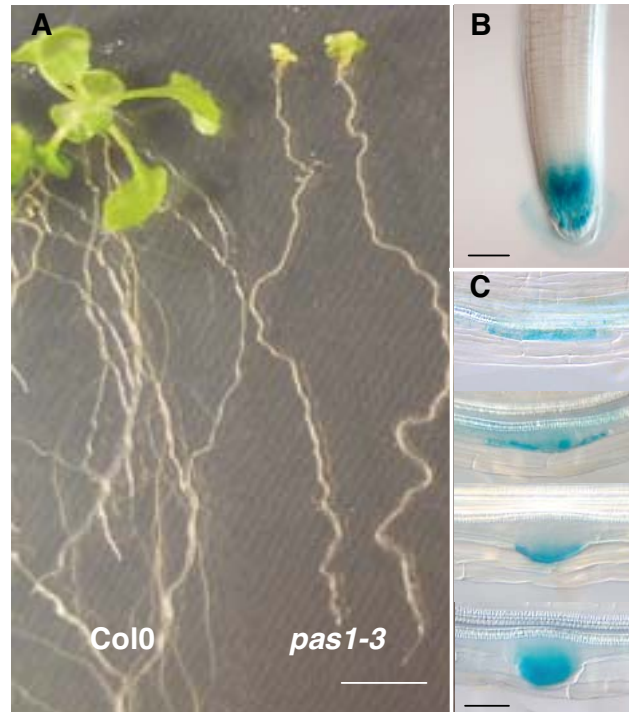


Supplemental Figure 8. Auxin accumulation and PIN1 polar distribution are altered in *pas3* embryo.

(A) *pDR5:GFP* expression in *pas3-1* mutant.

(B-E) Immunolocalization of PIN1. Comparison of PIN1 distribution between wild-type (B) and *pas3-1* mutant (C). Detail of PIN1 distribution in the tip of a wild-type cotyledon (D) and *pas3-1* embryo apex (E).

Bars, 40 μm (A, B, H); 20 μm (C, I); 10 μm (D,E); 2 mm (F), 5 μm (G).

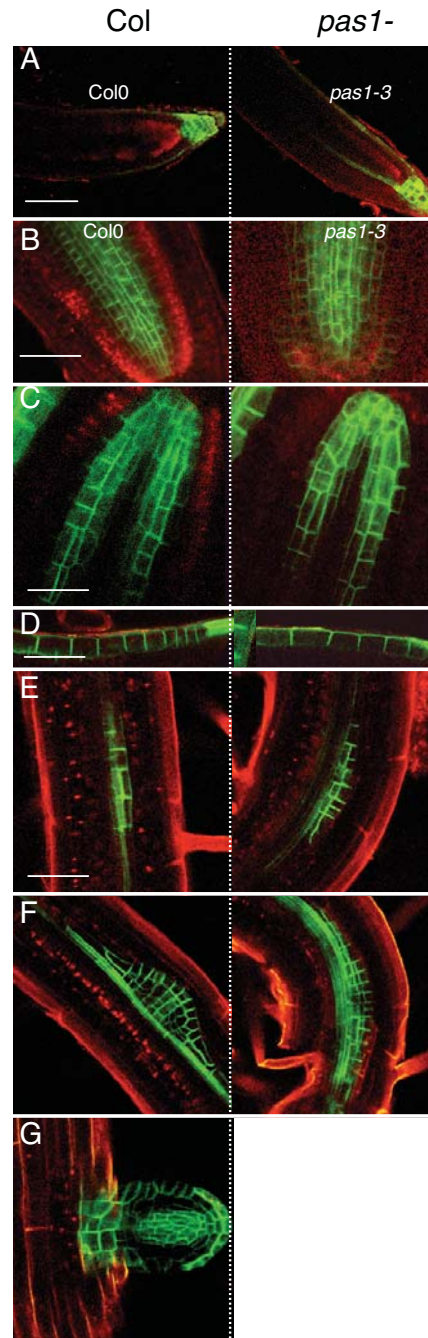


Supplemental Figure 9. PAS1 is involved in lateral root development.

(A) Lateral root development is inhibited in *pas1-3* mutant. Bar, 5 mm.

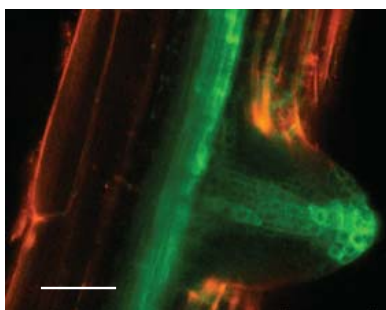
(B) *pPASI:GUS* expression in wild type primary root is restricted to the meristem and the columella cells. Bar, 70 μm .

(C) *pPASI:GUS* expression during lateral root initiation in wild type seedlings. Different stage of lateral root development are shown from the first pericycle divisions (top) to root outgrowth (bottom). Bar, 40 μm .



Supplemental Figure 10. Polar auxin transport during *pas1* root development.

- (A) *pDR5:GFP* expression in wild-type (left) and *pas1-3* in primary root (right).
 (B) *pPIN1:PIN1-GFP* expression in wild-type (left) and *pas1-3* in primary root (right)
 (C) *pAUX1:AUX1-YFP* expression in primary root protophloem (in wild-type (left) and *pas1-3* in primary root (right).
 (D) *pAUX1:AUX1-YFP* expression in primary root epidermis (in wild-type (left) and *pas1-3* in primary root (right).
 (E-G) *pAUX1:AUX1-YFP* expression during lateral root development in wild-type (left) and *pas1-3* in primary root (right). The *pas1-3* mutant never showed any lateral root outgrowth like observed in wild type (G)
 Bars, 70 μm (A); 45 μm (B); 20 μm (C, D); 45 μm (E - G).



Supplemental Figure 11. *pDR5:GFP* expression in emerging lateral root of wild-type seedlings . Bar is 35 μ m.

Supplemental Table 1. Relative sterol and sterol glycoside levels in *pas1* and *pas3* mutants

	Col 0	<i>pas1-3</i>	<i>pas3-1</i>
Sterols	10.8 ± 1.1 (n=5)	16.1 ± 1.9 (n=5)	14.2 ± 1.8 (n=3)
Sterol-glycosides	5.2 ± 1.1 (n=5)	5.4 ± 1.9 (n=5)	6.4 ± 1.8 (n=3)

Sterols and Sterol-glycosides are expressed as % of total lipid mass. Each value is the mean of several experiments (n) ±SEM.